Interhemispheric Comparison of Atmospheric Circulation Features as Evaluated from NIMBUS Satellite Data

Annual Report

Grant NGR 06-002-098

1 April 1970 - 30 June 1971

DEPARTMENT OF ATMOSPHERIC SCIENCE
COLORADO STATE UNIVERSITY
FORT COLLINS, COLORADO

ANNUAL REPORT

for

Grant NGR 06-002-098

E. R. Reiter, Principal Investigator

1 April 1970 - 30 June 1971

Prepared by

E. R. Reiter, T. H. Vonder Haar, J. E. Lovill

R. Adler, S. Srivatsangam and R. Abbey

Department of Atmospheric Science

Colorado State University

for

National Aeronautics and Space Administration

Contracting Officer: J. B. Jishow

Technical Monitor: V. V. Salomonson

CONTENTS

Summary

This Annual Report contains the highlights of our findings using IRIS data from NIMBUS III in mapping the global ozone distribution. The seasonal and regional variations of ozone, especially in the Southern Hemisphere, reveal note-worthy features that were not evident so far from the sparse ground-based ozone observation network in this hemisphere.

The regression of temperature and height fields on radiance data re-reals promising first results that will be expanded into a detailed study. With the aide of such satellite data we hope to obtain more quantitative indications of the differences in jet stream structure and in the energetics of the two hemispheres.

Spectrum analyses of upper wind data from the North American Section and from Australia have been completed. The results from this study will be useful when the representativeness of certain features of atmospheric flow obtained from specific geographic regions has to be assessed.

1.0 Introduction

In recent years the data provided by meteorological satellites have swelled into a steady stream of information that allows much more sophisticated assessments of the state of the atmosphere than a mere estimate of cloud cover. Especially the infrared experiments carried by the NIMBUS satellite series were designed to provide an insight into the vertical temperature structure of the atmosphere from which, by applying basic dynamical principles, one may derive large-scale flow patterns over wide regions of the globe.

With such a capability to depict atmospheric circulation features by remote sensing techniques one may attempt to map details of flow behavior over the vast regions of the Southern Hemisphere that are almost void of routine upper-air observations. The primary focal point for the present investigation has been to provide such circulation details for the Southern Hemisphere, using the IRIS data from NIMBUS III and IV.

Since satellite data will have to be calibrated against conventional meteorological measurements, our study could not be restricted to the Southern Hemisphere. Northern Hemisphere radiosonde and rawinsonde information, therefore, figures prominently as a formulation of our analyses.

Whereas our previous Semiannual Report (Reiter, et al, 1970) could report only moderate progress due to delays in the receipt of satellite data, the present report highlights several important conclusions, mainly from the ozone work that has been in progress.

To this date, one M.S. thesis (Mr. R. Abbey) has been finished in draft form. Mr. Abbey's investigation deals with spectrum analysis of upper-wind data in the jet-stream region and is intended as a statistical

background study against which satellite data analyses may be compared. This study has in part been supported by NASA Grant NGR 06-002-098. Mr. J. Lovill has finished the major portion of his Ph.D. dissertation, dealing with detailed ozone distribution in both hemispheres, as obtained from NIMBUS data. Mr. S. Srivatsangam is making considerable progress in establishing regression methods for estimates of temperature and height fields from satellite radiance data. This work hopefully will yield, in time, a Ph.D. dissertation. Atmospheric energetics in both hemispheres, based upon satellite information, is the topic of one investigation by Mr. R. Adler, also a Ph.D. candidate.

In the following paragraphs a short resume is given of ongoing work. In view of the forthcoming detailed reports by Messrs. Abbey and Lovill this summary report confines itself to a listing of essential findings.

2.1 Use of Ozone to Study Atmospheric Transport Processes

Prabhakara of GSFC developed regression techniques to arrive at the total O_3 content of an atmospheric column from radiance measurements. His data provided by GSFC on magnetic tape for 83 days out of a 90-day period (April-July 1969), were analyzed objectively at Colorado State University using computer programs that were discussed in our Semiannual Report (Reiter, et al, 1970). Extensive comparisons between satellite ozone data and ground based observations of total ozone were made. Mr. Lovill's Ph.D. dissertation deals with these ozone studies in great detail.

2.11 Meridional Gradients of O_3 Near Jet Maximum

Reiter (1971) summarized past research work on the ozone distribution in the atmosphere that could be derived from ozone soundings, aircraft measurements and ground-based umkehr techniques. From these studies it becomes quite obvious that the dynamically induced vertical motions associated with jet maxima near the tropopause extend into the lower stratosphere and induce an appreciable vertical transport of ozone. Specifically, it was found that the stratospheric air on the cyclonic side of the jet stream, which is subject to sinking motion, abounds in O_3 concentration; whereas the warm area in the jet core and on the anticyclonic side of the jet maxima, being of tropospheric origin, is deficient in ozone concentration. Since the ozone surplus on the cyclonic side, as well as the deficit on the anticyclonic side, extends over a considerable depth of the atmosphere, one would expect to find a marked horizontal gradient of total O_3 to be present across the axes of well-developed jet streams.

Thirty-three cases of relatively sharp meridional gradients of total O_3 in the Northern Hemisphere on the objectively analyzed charts of O_3 as observed by NIMBUS III, have been tested with respect to the presence or obsence of jet maxima. Not only did we find a strong correlation between such gradients of O_3 and the proximity of jet stream, but the magnitude of these gradients appeared to stand in direct relationship with the intensity of the jet stream, i.e., with the peak wind speeds observed in its case. This is illustrated in Figure 2.11.1. Numbers in the diagram identify the individual cases of the study.

One individual case, of 7 May 1969, is illustrated further in Figure 2.11.2. A strong Pacific cyclone and its associated jet are shown superimposed on an objective analysis of the IRIS ozone values. Maxima and minima of O_3 correspond well with the postulated vertical motion fields near the jet core.

We will attempt to apply the correlation outlined in Figure 2.11.1 to ozone concentrations in the Southern Hemisphere where upper-wind data are sparse.

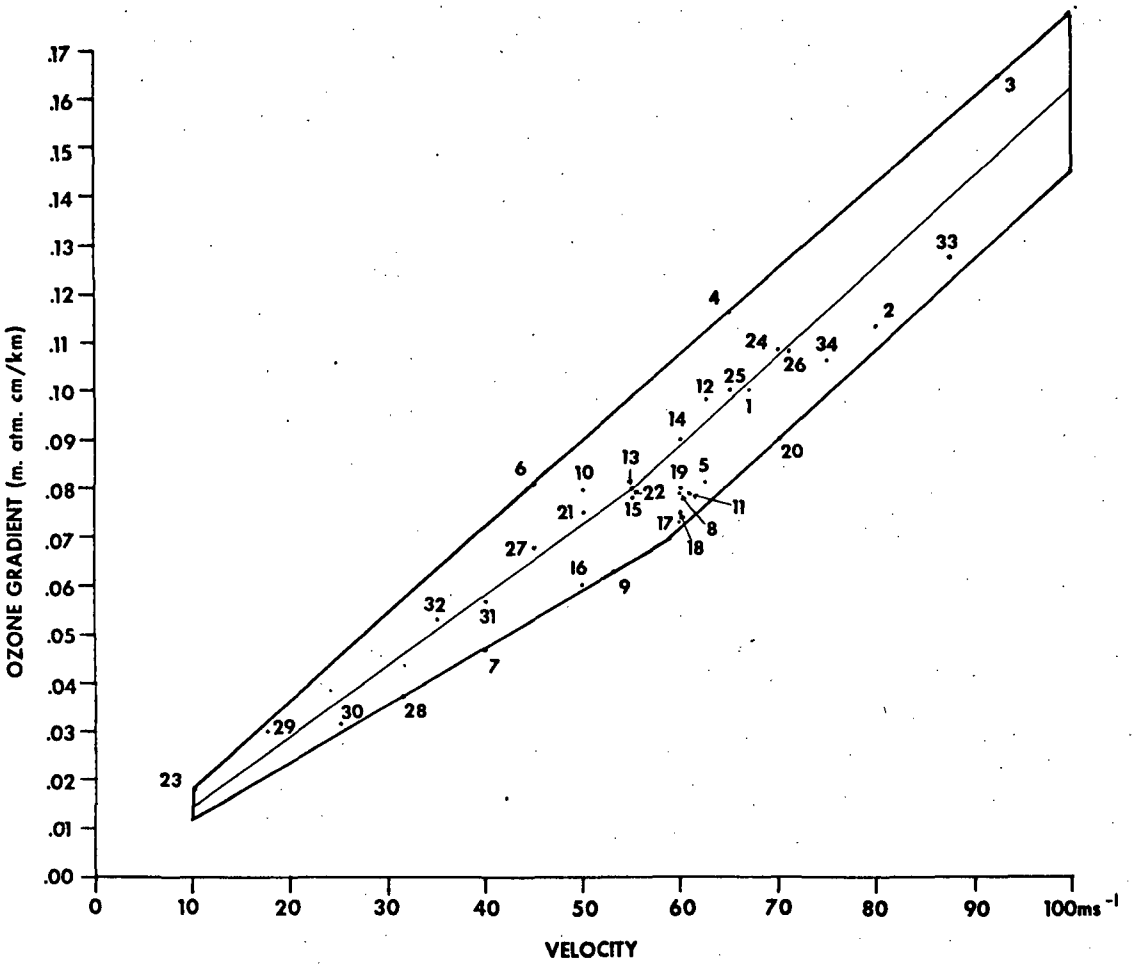

Fig. 2.11.1 Graph of the non-linear relation between total ozone gradient (in m·atm·cm/km) and the jet stream core velocity (in ms^{-1}).

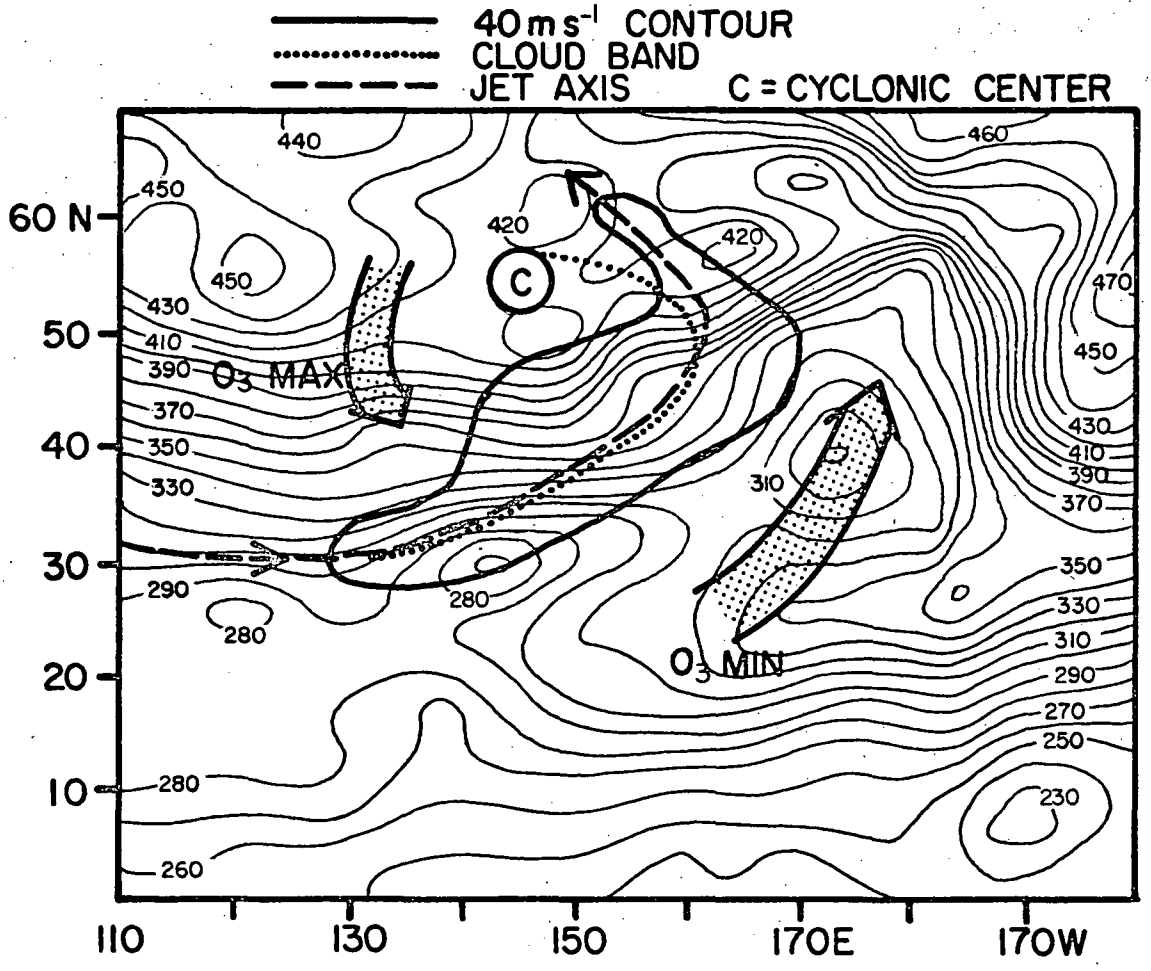

Fig. 2.11.2 Overlay of the wind velocity and cyclone cloud band on an analysis of the meso-scale total ozone distribution.

2.12 Global Ozone Climatology: Temporal and Geographical Variations

Dynamically induced subsiding motions, in combination with strong horizontal advection, behind a short-wave trough could produce large positive changes in the total ozone concentration over an extensive area. As was illustrated in Figure 2.11.2, the ozone concentration decreases rather markedly on the west side of a ridge: With these correlations we can inspect longer term temporal and geographical variations of ozone on a quasi-seasonal basis. Many general circulation characteristics may thus be portrayed by the ozone distribution.

2.12.1 Northern and Southern Hemisphere Comparisons

Several studies in recent years have shown distinct differences of the atmospheric general circulation of the Northern and Southern Hemispheres (for a summary, see Reiter, 1969). Whereas, earlier publications postulated a more zonal flow in the Southern Hemisphere supposedly because of less land mass and fewer mountain massifs, more recent investigations show that such statements may have to be qualified somewhat.

Wooldridge and Reiter (1970) have shown that significantly stronger horizontal anisotropy of flow prevails at cyclone wavelengths in the Southern than the Northern Hemisphere, with meridional perturbations exceeding zonal flow perturbations. Eulerian spectral densities of the zonal component in the Southern Hemisphere were half of those in the Northern Hemisphere. This would imply that there is less energy at cyclone-wave frequencies in the Southern than in the Northern Hemisphere. Wooldridge and Reiter (1970) suggest that this occurs because of a relative lack of orographically induced planetary longwaves in the Southern Hemisphere that are superimposed upon the hemispheric jet stream zones. They concluded that the relatively zonal character of the

Southern Hemisphere pertains to the long planetary-scale waves only.

Starr and Dickinson (1963) have shown that standing eddies are very important in transport processes of the Northern Hemisphere. Obasi (1963a) pointed out that transient eddy processes are of utmost importance in the flux of momentum toward the pole in the Southern Hemisphere. Obasi (1963b) also found that the conversion of eddy kinetic to zonal kinetic energy by such waves was about twice as great in the Southern Hemisphere as in the Northern Hemisphere.

These studies imply that transport processes in the Southern Hemisphere depend more on the cyclone scale disturbances than in the Northern Hemisphere. In the Northern Hemisphere much transport is associated with standing eddies which have wave numbers of 1, 2, and 3.

Jet stream patterns in the Northern Hemisphere are strongly influenced by the hemispheric wave number three (Reiter, 1963). This results in the formation of the three strongest mean jet maxima over Japan, Eastern North America, and Europe, (Kao and Hurley, 1962). On the average these jet stream systems are stronger in the Northern Hemisphere winter than in the summer.

In the Southern Hemisphere Van Loon (1964, 1965) finds a differently structured jet stream system: In winter, the zonal momentum is greatest. The momentum is distributed over <u>two</u> hemispheric jet stream systems. In the Southern Hemisphere summer only <u>one</u> jet stream system is reported (over the Indian Ocean) by Van Loon (1964). This single jet maximum has a <u>greater</u> velocity than either of the two jet maxima observed during the winter in the Southern Hemisphere.

Large-scale circulation patterns also show a disparity between the Northern and Southern Hemispheres. Planetary waves number two and three

shape the polar vortex in the Northern Hemisphere winter. In the stratosphere, the circulation is such that upward motion is seen over the North Polar Regions during the late winter during and after the breakdowns of the stratospheric polar vortex (Reed et al., 1963; Teweles, 1964). Subsiding motions are wide-spread over the middle latitudes (Reiter, 1969). Since ascending currents dominate in the equatorial regions, the general circulation of the stratosphere is accomplished by two cells which produce an observed spring maximum of ozone in middle and high latitudes of the Northern Hemisphere (Reiter, 1971). London (1963) in a state-of-the art paper presented seasonal and annual mean charts of total ozone data from sixty stations, most of which were in the Northern Hemisphere. He found in both the seasonal and annual means that three ozone maxima were evident in troughs extending from the high latitudes toward the equatoral regions. These waves in the ozone isolines conformed quite closely to the troughs in the stratospheric circulation pattern.

2.122 Inter-hemispherical Comparisons of Monthly Ozone Variability

Figures 2.122.1a to 2.122.1d represent Spline Function computer analyses of Northern Hemispheric total ozone data and Figures 2.122.2a to 2.122.2d show similar analyses for the Southern Hemisphere. The charts for April represent the last twelve days of the month and the analyses for July, the first twenty-one days of the month. More data were available for analysis in the Southern than the Northern Hemisphere. For example in May in the Northern Hemisphere 22,519 points were analyzed. In the Southern Hemisphere 30,110 data points were available - an increase of 25%. This deficiency of points in the Northern Hemisphere is mostly a function of data retrieval from the satellite at the two acquisition stations. All

orbits cannot be recovered owing to memory storage on the satellite and an insufficiently rapid data bit transmission from the spacecraft to the station.

2.123 A Detailed Study of April in the Northern Hemisphere

Figure 2.122.1a shows the mean total ozone distribution for April in the Northern Hemisphere. Two features are obvious in this figure: (1) a 'tight' ozone gradient extends from Eastern North America to about 60^{o} W in the western part of the Atlantic Ocean, and over Eastern Asia and Japan; (2) There are four to five major waves in the ozone isolines.

An analysis of the National Meteorological Center (NMC) upper troposphere and lower stratosphere wind data indicates that the two regions with closely spaced ozone isolines coincide with the average location of strong baroclinic zones. The 'tight' gradient of mean total ozone concentration seems to be directly identifiable with the mean position of strong polar jet stream systems.

Four or five long waves also can be identified in the ozone isoline pattern. These ozone ridges (maxima) and troughs (minima) correspond closely to long-wave features found in the height contour fields at 300 to 100 mb. Shorter, transient total ozone waves tend to be filtered out in the averaging process used to obtain monthly means. Several of these short-wave features are evident in this "April" map (Fig. 2.122.1a) however, since only twelve days of data were averaged. The other months have two to three times as many days to average, and thus identify mostly standing wave features.

In Figure 2.122.1a the areas from the 300 m·stm·cm total ozone isoline northward (southward in the Southern Hemisphere; see subsequent diagrams) to the thirty degree latitude line are widely dotted to indicate pre-

ferred global regions of southward total ozone transport by the standing, long planetary waves. The finely dotted areas from the 300 m·atm·cm isoline southward (northward in the Southern Hemisphere) to the thirty degree latitude line represent preferred global regions of northward total ozone transport. A large region over which the 300 m·atm·cm line is displaced north of 30° N extends from Central Asia to Western Japan. With the exception of slight displacements to the north over Iran and Arabia and the Mid-Atlantic, the remaining area of the Northern Hemisphere has the 300 m·atm·cm isoline displaced to the south of 30°N. This implies that a larger amount of ozone is advected southward of 30°N than is advected northward at this time of the year. The orientation of the 300 m·atm·cm contour is mostly a function of the standing planetary wave system and the resulting subsiding (ascending) and southward (northward) mass transport which results in preferred regions of total ozone maxima (minima). The average concentration of ozone along a latitude circle, however, is mostly a function of the zenith angle of the sun.

The 260 m·atm·cm contour for the months of April-June, and the 280 m·atm·cm contour for July have been marked especially, to emphasize preferred regions where ozone maxima exist in the tropics. In April (Figure 2.122.1a) the 260 m·atm·cm contour tips far south and generally intercepts the equator over much of North Africa.

In May, June, and July (Figures 2.122.1b, c, d) a very 'tight' ozone gradient is evident again over Eastern North America. It is worthy to note that this area of concentrated ozone contours has moved a considerable distance northward from April to July. In April the average value of total ozone off the east cost of North America at 45° N was 400 m·atm·cm.

By July the value at this location had decreased to 340 m·atm·cm. This seems to correlate reasonably well with the weakening and movement toward the north of the baroclinic zones. The tightly packed ozone contours seen over Central Asia and Japan in April appear to persist through July, but with considerable weakening after June over Japan. By comparison the gradient over Eastern North America is several times that of the gradient over Japan in July, but about equal to that found over Eastern Asia. Even though there are four standing planetary waves in July indicated in the height contour field (Scherhag, 1969a) and in the ozone contour field (Figure 2.122.1d), it appears as though much of the jet-stream activity is concentrated over Eastern North America and Eastern Asia. The ozone gradients over the rest of the Northern Hemisphere are considerably less than over these two regions.

Scherhag (1969b) reports that the average wind velocity for several Japanese stations between 35 to 40° N at longitude 135° E for May at 200 mb was 40 ms^{-1}. The total ozone gradient in this region, using Figure 2.122.1b, was 0.54 in atm cu/km. Using Figure 2.11.1 correlating ozone gradient and jet stream winds, we arrive at an estimated velocity of 37 ms^{-1}. This is in good agreement with the actually measured winds, even though the wind reports pertain to 200 mb, and the correlation chart was developed for use at 250 mb.

From April to July in the Northern Hemisphere (Figure 2.122.1a-d) there are three to five long waves visible in the total ozone contours. The month of June is the only month with a dominant three wave pattern. A closed center of ozone concentration appears in high latitudes at approximately 175° E longitude. A dominate feature on the 200 mb mean June contour map is a closed warm center west of Alaska in the same location as the closed ozone contours (Scherhag, 1969b). This feature re-

mained quasi-stationary during June and appears to have influenced rather markedly the upper atmospheric flow over Western North America and Northeast Asia.

In April we found most of the 300 m·atm·cm contour to the south of latitude 30°N. By July (Figure 2.122.1d) much of this contour lies to the north of this latitude. The months in-between represent a transition period during which the general circulation in the Northern Hemisphere is in a state of decreasing kinetic energy and during which most centers of action have shifted northward.

Several interesting temporal variations of ozone at different geographical locations are worth mentioning. One of these locations is the United States. In April the 300 m·atm·cm contours extended to about 20° N in the longitude sector of the United States. But in May a small portion of this contour is noted pushing northward across 30°N over Texas. In june this area has enlarged to cover most of the south-central United States. By July a greater part of the United States has an ozone concentration of less than 300 m·atm·cm. This feature appears to represent an event that increases steadily in time an import of lesser values of ozone northward into an area centered on the 95th meridian. A region off the east coast of the United States, during April showed a northward indentation of 300 m·atm·cm line, and in July was seen to be a preferred region for a southward bulge of this contour line.

There was only one region in the Northern Hemisphere where the 300 m·atm·cm contour remained north of the 30°N latitude during all four months. This was the region from Central Asia to Japan. The area over which there was very little seasonal ozone variability at 30°N was from western North Africa to Iran (15°W to 60°E).

The 260 m·atm·cm contour in April, May, and June (280 m·atm·cm in July) characterizes the ozone distribution in tropical latitudes. Relatively high values of O_3 appear over Africa and the Eastern Atlantic Ocean. The departures from zonal mean values are not strong, but nevertheless suggest the possibility that this is a preferred region ($3^{\circ}W$ to $60^{\circ}E$) for interhemispherical exchange of stratospheric air masses.

In general it appears that the western part of the Northern Hemisphere has the greatest seasonal variability of total ozone and that the eastern part has the least variability.

2.124 Monthly Southern Hemisphere Variability

There are a total of eleven active ozone surface stations in the entire Southern Hemisphere. As a contrast, the United States and Canada alone have thirteen stations. Of these eleven Southern Hemispheric stations there are four between the equator and 30°S, five between 30°S and 60°S, and two from 60°S to the pole. With a network as thin as this only a very basic understanding of the ozoneosphere in the Southern Hemisphere exists and this has primarily come from the Australian network of five stations. The following maps (Figures 2.122.2a-d) are a first look at the longitudinal variations, the long-wave isoline pattern, and the gradient of total ozone in the Southern Hemisphere.

In April a 'tight' gradient is located approximately along the 100th Meridian between 40 and 50°S. This gradient weakens considerably in May but reappears nearly as strong in June and July. In May there are two regions of strong meridional O_3 gradients -- one over the Eastern Atlantic and the other over Eastern Indian Oceans. The gradients over both these regions are somewhat less than the gradient southwest of Australia mentioned above. In June the strong gradient southwest of Australia is again evident, as in another region of tightly-spaced contours in the south central Pacific Ocean. In July we find both of the features remaining in essentially the same locations. Van Loon (1964) reports a broad westerly wind maximum at 45-50°S from 45-100°E. This is in more-or-less general agreement with the ozone gradients in this region.

The gradient southwest of Australia is nearly as strong in April as it is three months later in July, the middle of the Southern Hemisphere

winter. One might infer from this that the jet stream system over this region is nearly of the same velocity in the late summer as in the middle of winter. This would support the statements of Southern Hemispheric jet streams made in Chapter 2.121. The ozone contours indicate that the jet stream moves slowly northward from April to July as observed from wind analyses.

In the Southern Hemisphere from April to July the ozone isoline pattern is arranged in a pattern of four to five planetary waves. This is similar to the wave pattern we observed in the Northern Hemisphere. At least for the four months discussed in this paper, there appears to be four 'anchor' locations for the "ozone troughs": 100^{o}E, 175^{o}W, 100^{o}W, and a broad area in the South Atlantic. The latter location is ill-defined and variable on all mean maps.

In April we see essentially that all of the 300 m·atm·cm contour is south of 30^{o}S. The only exceptions to this are small areas over south central Australia and in the south central Pacific. This pattern appears to be typical for the Southern Hemisphere in early fall. The variation in the oscillation of the 300 m·atm·cm contour about latitude 30^{o}S is less in the Southern Hemisphere than in the Northern Hemisphere. Peculiar seasonal variations of total ozone are indicated over Australia. In April a small positive anomaly is found over this continent. In May this small area of maximum ozone has expanded and now covers over half of the width of the continent (Figure 2.122.2b). By June the extension is complete and the 300 m·atm·cm contour lies north of 30^{o}S over the entire

continent. In July the positive anomaly shrinks slightly, but extends further westward. During this entire period (April to July) the total ozone at 105°E and 30°S has shown in essence no variance. The increase of total ozone over Australia, as winter approaches, seems to correspond to a decrease of total ozone over the North American Continent as summer approaches.

One other area with an anomalous maximum should be noted. In May the 300 m·atm·cm contour has a slight 'bulge' to the north of 30°S off the west coast of South America (Figure 2.122.2b). By July this maximum has extended to 20°S and covers all of the extreme southern part of South America. A final region noteworthy of mention is the western part of the Indian Ocean. Over this entire region an ozone minimum is reflected in the 300 m·atm·cm contour.

The 260 m·atm·cm contour in April, May, and June (280 m·atm·cm in July) indicates relative high total ozone concentrations in the tropical latitudes over Africa and the Eastern Atlantic Ocean.

Basic similarities of the distribution of total ozone in the Northern and Southern Hemispheres are the following: Both hemispheres show: (1) a preference for a four wave ozone pattern; (2) 'tight' ozone gradients which, we hypothesized, are directly related to jet stream system; (3) a general increase (decrease) of O_3 at a given latitude as we progress toward the winter (summer) season; (4) regions of relatively high ozone concentration in the tropics over the Eastern Atlantic Ocean and the African Continent.

Basic dissimilarities in the distribution of total ozone are the following: (1) whereas two and occasionally three regions of 'tight' ozone gradients were observed over the Northern Hemisphere, two and

sometimes only one such region could be seen over the Southern Hemisphere. This difference may partly be based on the fact that different seasons in each hemisphere are being compared. This should be remedied when NIMBUS IV data become available for a complete year; (2) there are larger variations of total ozone at a given latitude in the Northern Hemisphere. This may also be due to the out-of-phase seasonal comparisons.

2.125 The Variation of Total Ozone at 60°S for 20 Days in May 1969

Figure 2.125.1 shows a time-longitude distribution of total ozone for 60°S. This particular latitude was selected so that comparisons could be made with radiance values that were computed for the first two-thirds of May by Fritz (1970). Fritz's computations were for $\nu = 669.3\ cm^{-3}$. At this particular frequency he was measuring the radiance value of the high stratosphere. Ninety per cent of the flux which arrives at the satellite comes from above 100 mb (Fritz, 1970). This is a good frequency at which to observe and compare ozone variations, because it is centered in a region of the stratosphere between 20 and 50 mb in which a large percentage of the total ozone is concentrated.

Upon examination of Figure 2.125.1 several features are readily apparent. Both maxima and minima of ozone progress steadily to the east. Fritz describes the maxima and minima of radiance values as 'waves'. This seems to be appropriate here as well. These ozone 'waves' move in the same direction as the radiance 'waves' described by Fritz (1970). Fritz's low (high) radiance values correspond to low (high) stratospheric temperatures. His locations of high and low stratospheric temperatures are indicated by w and c, respectively, in Figure 2.125.1. Note that warm stratospheric temperatures correspond fairly well with high concentrations of ozone. Low ozone values seem to agree with cold stratospheric temperatures. This correspondence has been shown from earlier balloon-borne

ozonesonde packages (Craig, 1965; Lovill and Miller, 1968). The light lines sloping to the right with time are indications of the rate of eastward movement of the 'ozone waves'. Each line has a number associated with it. The average rate of longitude movement for each wave is indicated in Table 4.3.

Table 4.3

Eastward Progression Rate of Total Ozone 'Waves' at 60^{o}S for the Period 3-19 May 1969

Wave Number	Progression Rate (Degrees of Longitude/Day)	Average Concentration of Ozone Within Wave (m·atm·cm)
1	5.6	380
2	5.7	350
3	7.1	380
4	13.3	350
5	3.8	360

The variability of the longitudinal progression of these waves is quite large, ranging from 3.8 to 13.3 degrees longitude day $^{-1}$, with an average movement of 7 degrees longitude day $^{-1}$. Studies of this type should help relate stratospheric ozone variations to thermal fluctuations, and this in turn should promote a better understanding of the dynamics of the stratosphere.

2.126 Average Variation of Total Ozone with Latitude

Figure 2.126.1 represents the first attempt to describe the monthly total ozone distribution in the Southern Hemisphere. London (1963), basing his analysis on the ozone data available through 1959, arrived at an average curve for the spring that extended from the equator to the

North Pole. London had to extrapolate the curve south of 20°N and north of 75°N. His curve is plotted in Figure 2.126.1. Notice the remarkable agreement between his average curve for the spring and the average IRIS curves for April and May. The total number of ozone data points used to construct the April-July line was 1.8×10^5. Mean total ozone is given for the months of April, May, June, and July as well. Immediately evident from Figure 2.126.1 are increasing ozone values from the equatorial region to the poles in each month.

The largest gradient of total ozone is clearly found in the middle latitudes (35-50°N) in the Northern Hemisphere. The location of the steepest gradient in the Southern Hemisphere is not as well defined. Two preferred areas are indicated in the Southern Hemisphere. One is in the subtropics from 20-25°S. The other is from approximately 30-40°S. The former may be influenced by the change in regression coefficients used in the calculations. A slope of similar steepness, perhaps also somewhat biased by the regression coefficients, appears in the curve for April at 18-25°N.

Seasonal variation of total ozone is smallest in the tropics. In the Northern Hemisphere this occurs at 15°N, in the Southern Hemisphere at 20-30°S. The latter location may be influenced to a certain extent by the regression coefficient changeover, but nevertheless it is felt that the smallest variation is in this 20-30°S latitude band.

London (1963) found from the extrapolated data south of 20°N that the smallest ozone variations occurred at the equator. These variations amounted to approximately 4-5 m·atm·cm between summer and spring at the equator. However, Figure 2.126.1 indicates that at the equator, using data that have not been extrapolated, the variability from the spring

months (April and May) to the summer months (June and July) is 15 m·atm·cm.

Another interesting feature of the figure is that the minimum ozone values for all latitudes for all four months are between 5 and 10°S. It will be very interesting to see how this minimum migrates during the other months when NIMBUS IV data are analyzed.

In the Northern Hemisphere the total ozone in April reaches a peak at 70°N; this corresponds fairly well with London's (1963) winter peak at 60-65°N, but not at all with his curve for spring. In the Southern Hemisphere June and July have peaks at 68°S and 60°S, respectively. April has a secondary peak at 66°S and presumable another one south of 78°S. The unusual feature of an ozone minimum value at 70°S is difficult to explain unless it is due to an anomalous standing-wave situation near Antarctica.

Several important facts have been elaborated upon in Figure 2.126.1: (1) For the first time the average distribution of ozone with latitude has been determined by satellite for a period of several months; (2) the distribution agrees very well with the data from the long-term data base in the Northern Hemisphere; (3) the latitudinal ozone distribution, for the first time, has been described during the autumn and winter in the Southern Hemisphere; (4) the smallest variation of ozone from spring to summer was seen at 15°N. This did not agree with London's (1963) minimum of variation at the equator; (5) the lowest mean ozone value for the period was at 6°S.

2.127 The Global Distribution of Ozone from 19 April to 21 July 1969

Using 1.8×10^5 ozone data points, Figure 2.127.1 was constructed. The figure is the final product of a computer analysis using a two-dimension spline function.

Many of the features evident on this map have been discussed at length earlier in this section. The large region of maximum ozone in the tropics from the Atlantic Ocean eastward across Africa, that was discussed earlier, is more easily seen in this figure.

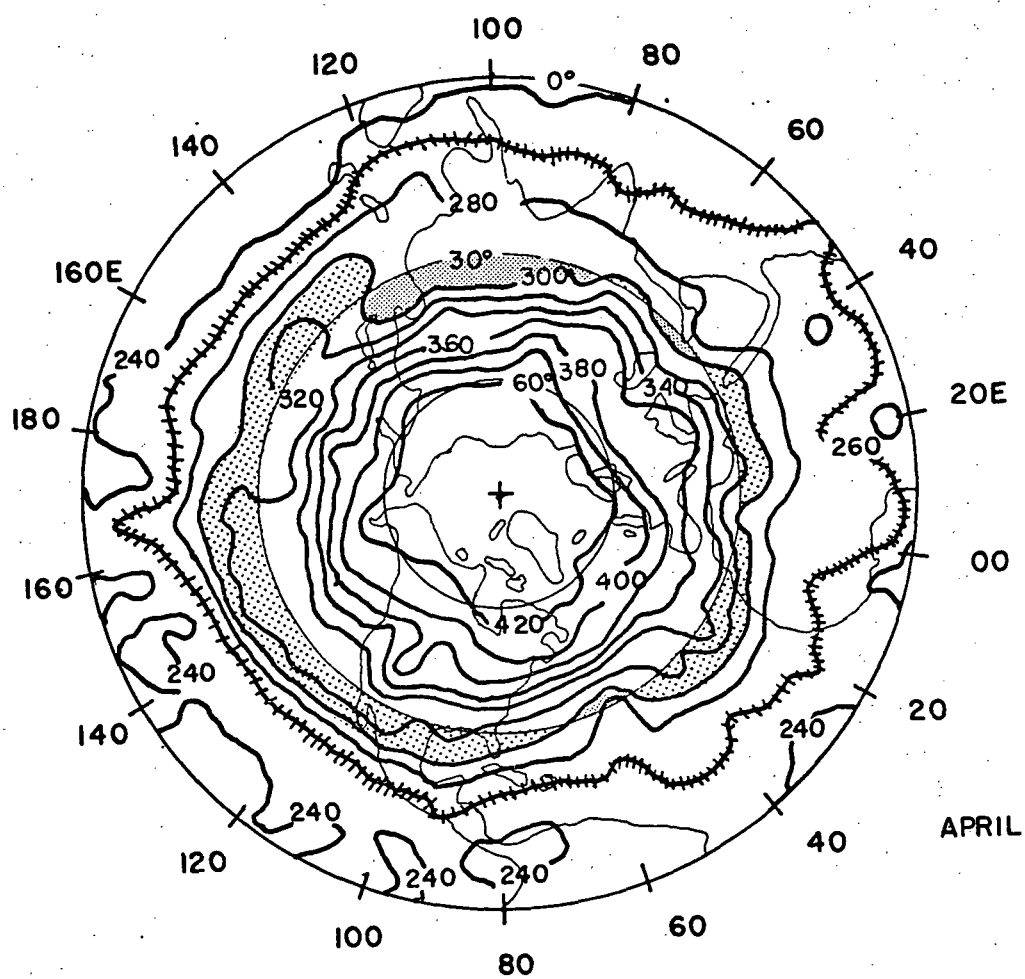

Fig. 2.122.1a Total ozone distribution in the Northern Hemisphere for April 1969. (This is a preliminary analysis of the satellite data. When final refinements of the data are published, changes may be produced in the ozone isoline analysis.)

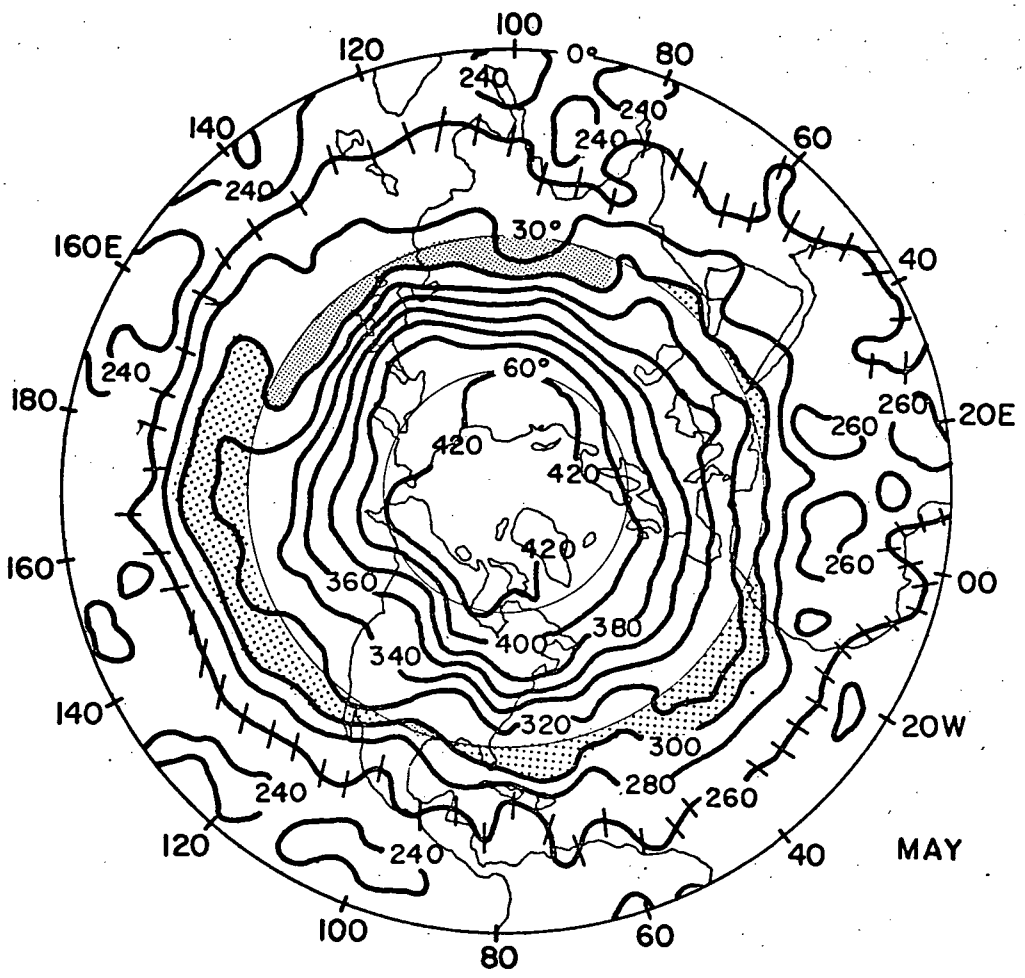

Fig. 2.122.1b Same as 2.122.1a except for May 1969.

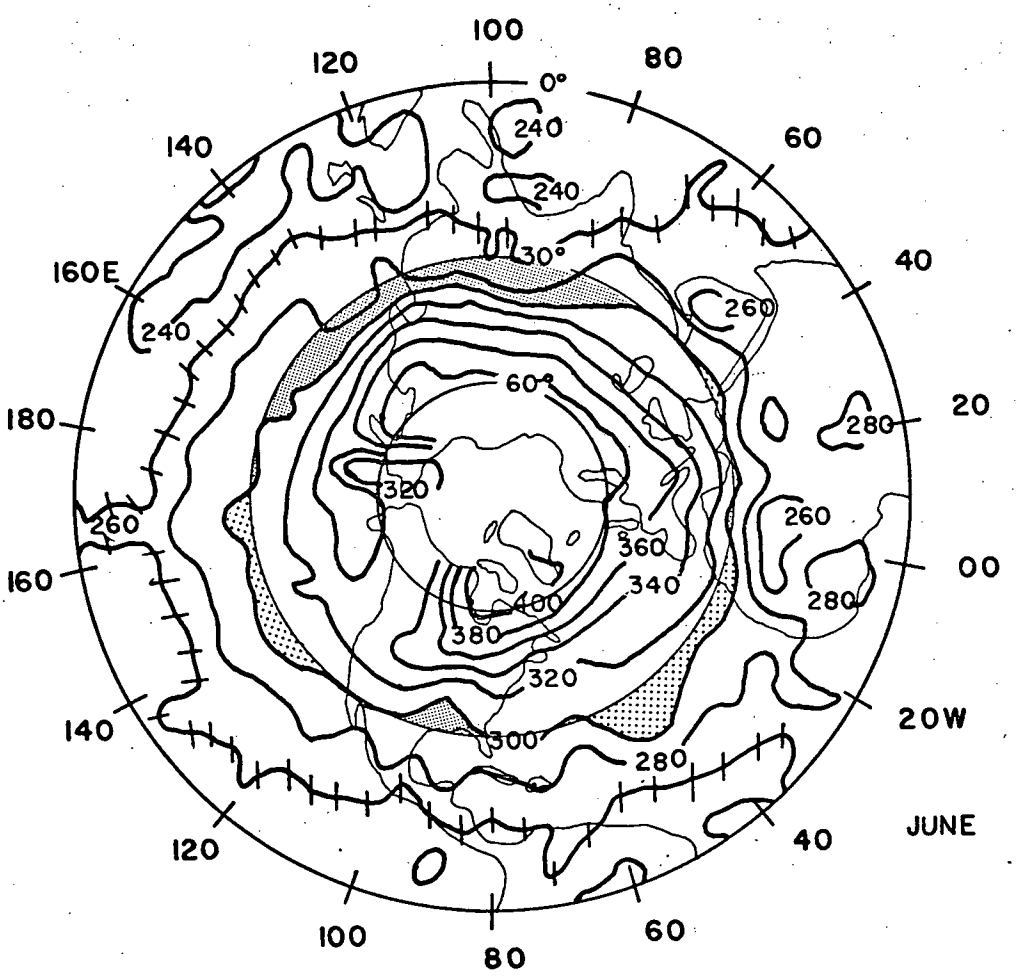

Fig. 2.122.1c Same as 2.122.1a except for June 1969.

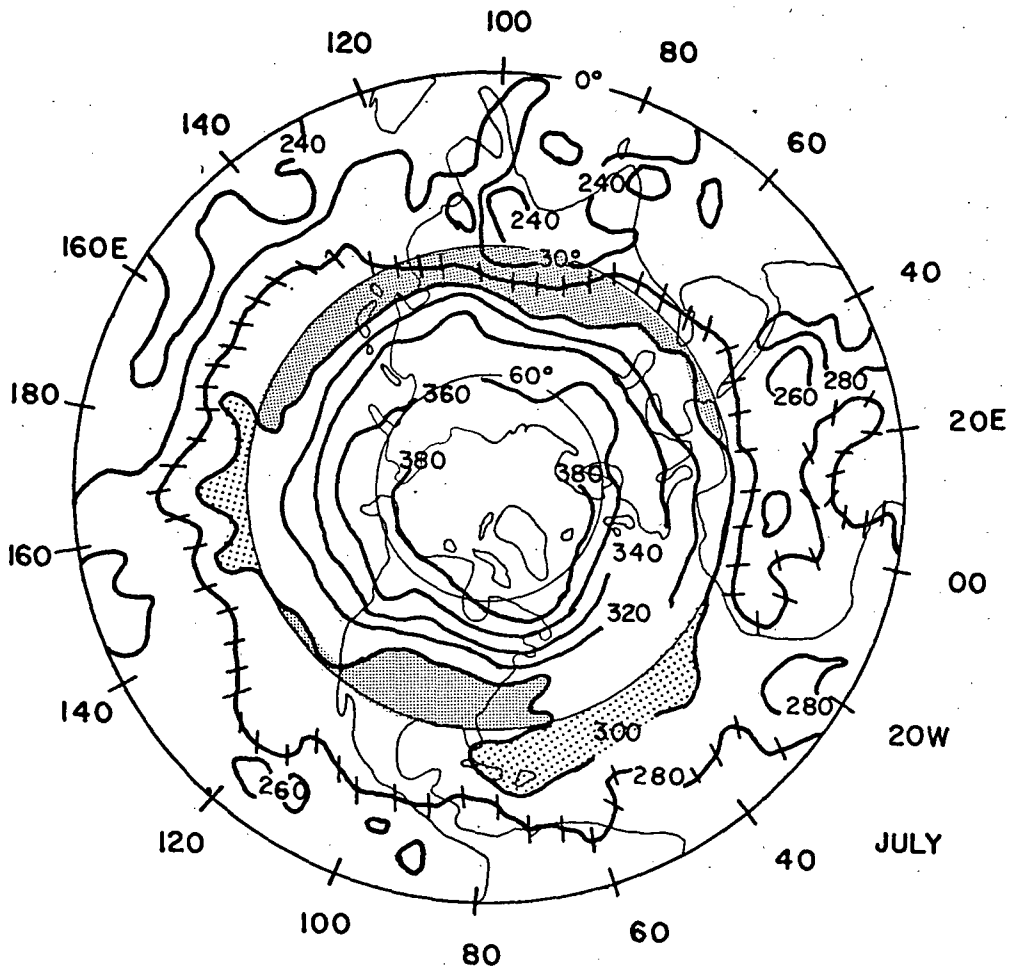

Fig. 2.122.1d Same as 2.122.1a except for July 1969.

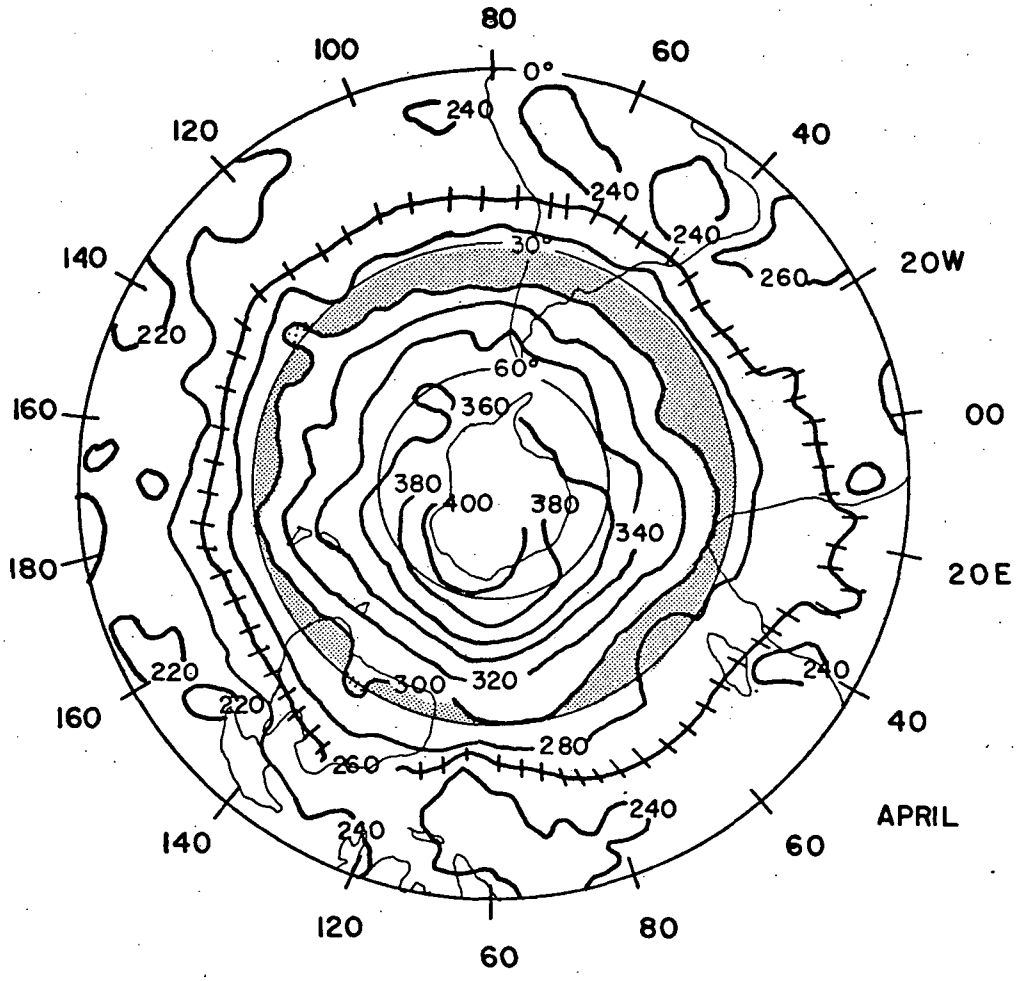

Fig. 2.122.2a Same as 2.122.1a except for April 1969, Southern Hemisphere.

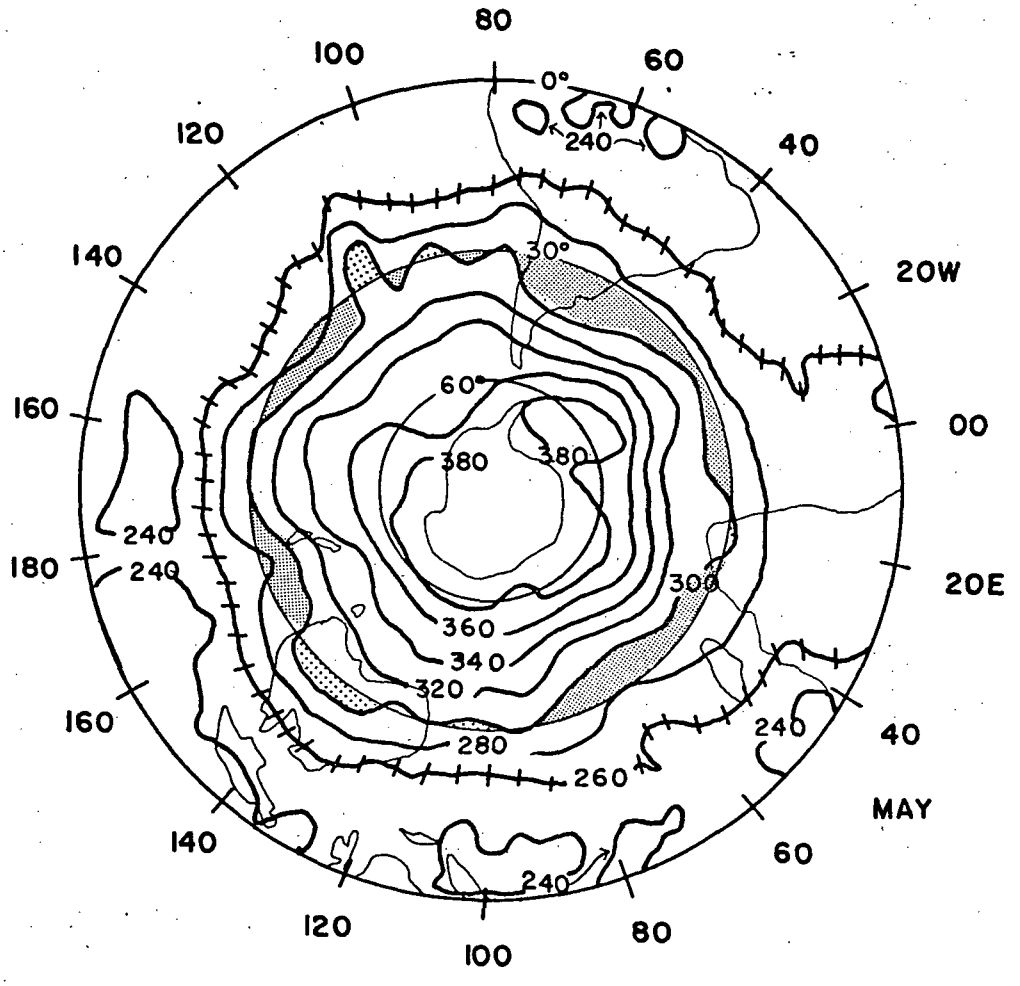

Fig. 2.122.2b Same as 2.122.1a except for May 1969, Southern Hemisphere.

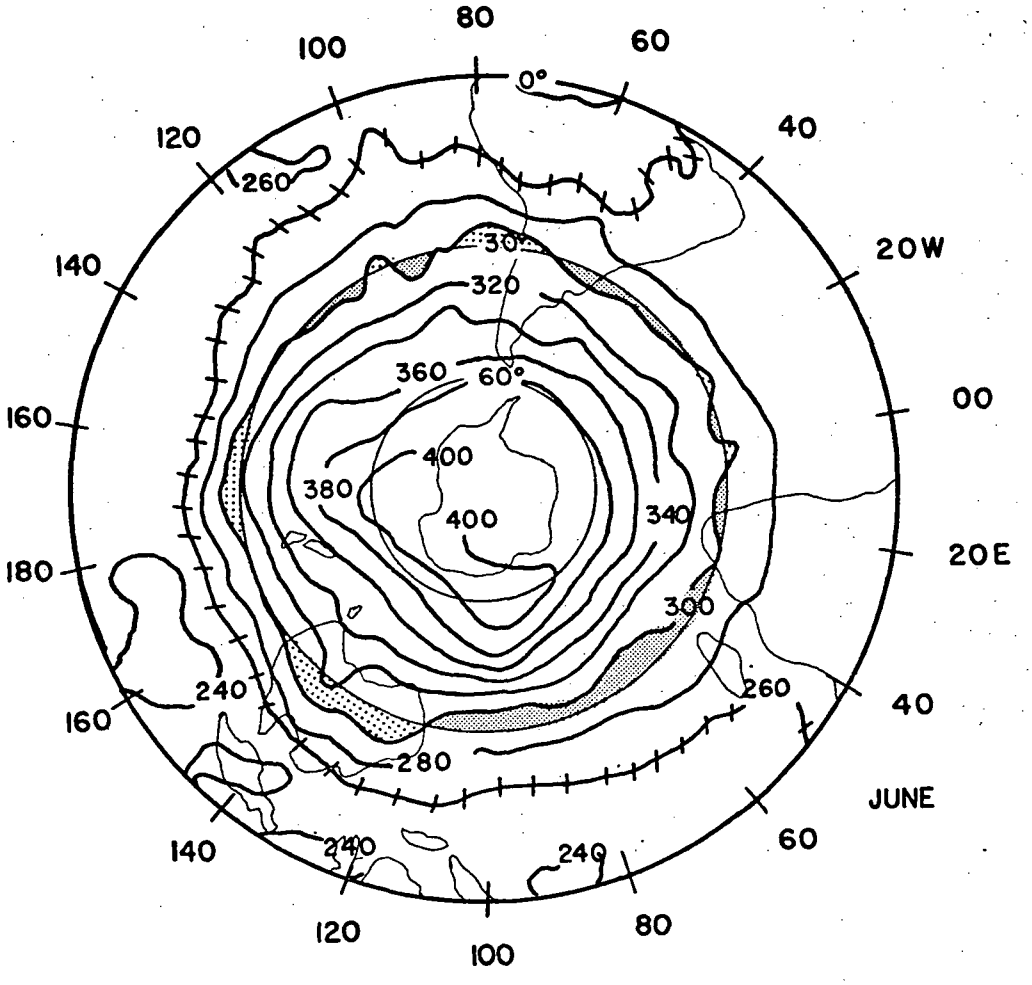

Fig. 2.122.2c Same as 2.122.1a except for June 1969, Southern Hemisphere.

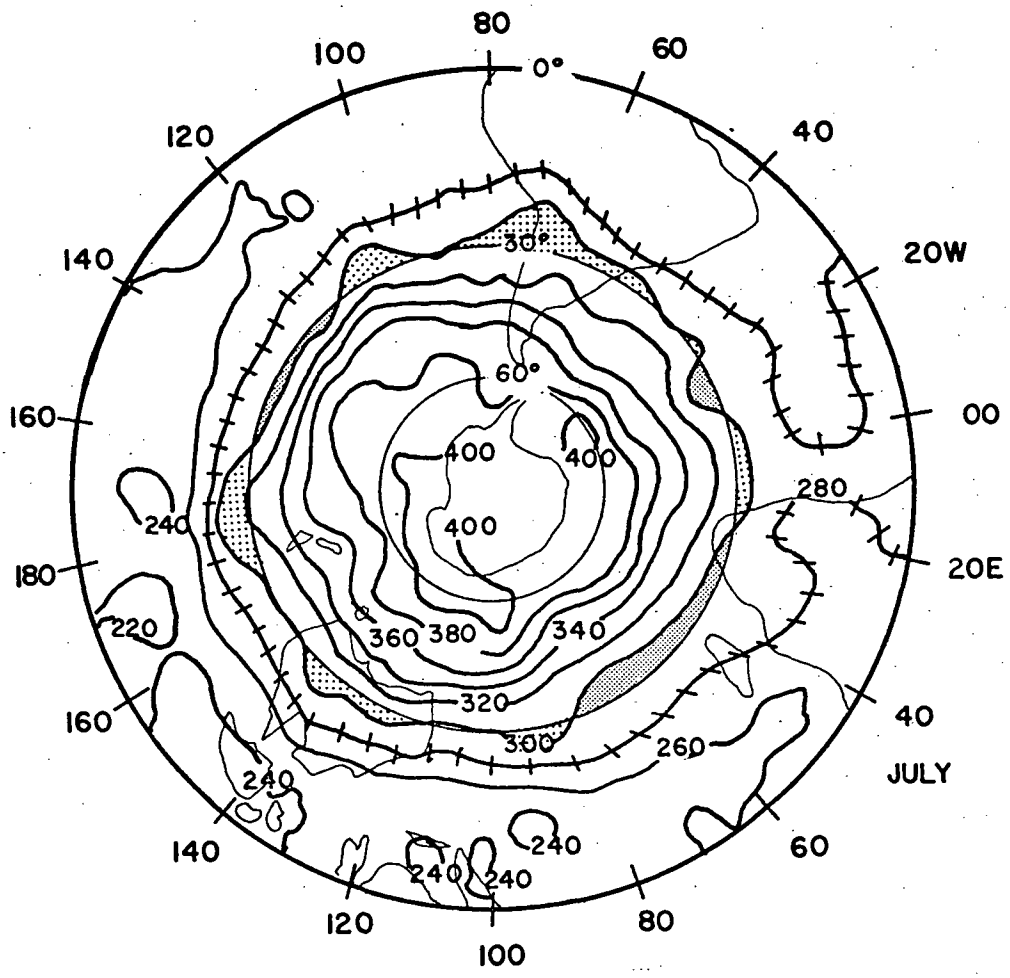

Fig. 2.122.2d Same as 2.122.1a except for July 1969, Southern Hemisphere.

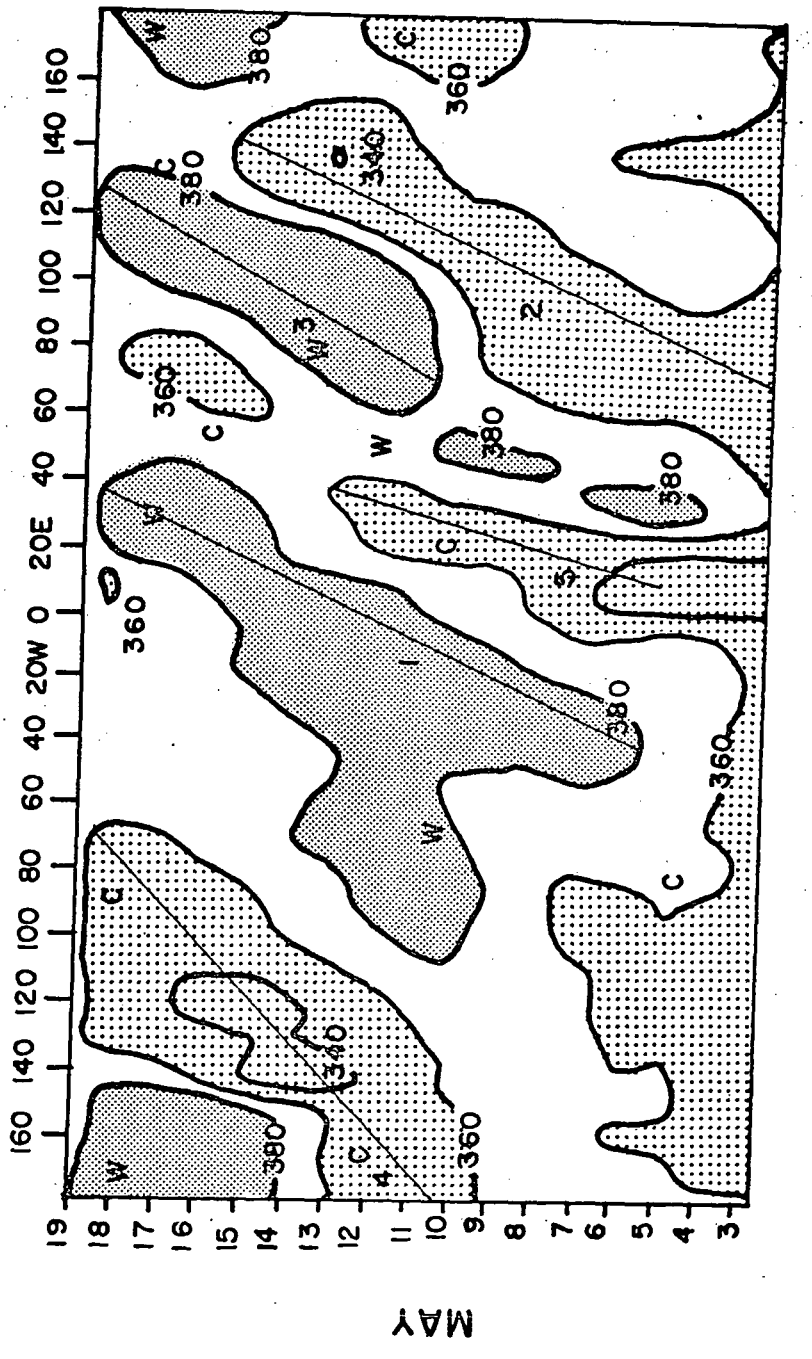

Fig. 2.125.1 Time-longitude graph of the total ozone at 60^{o}S.

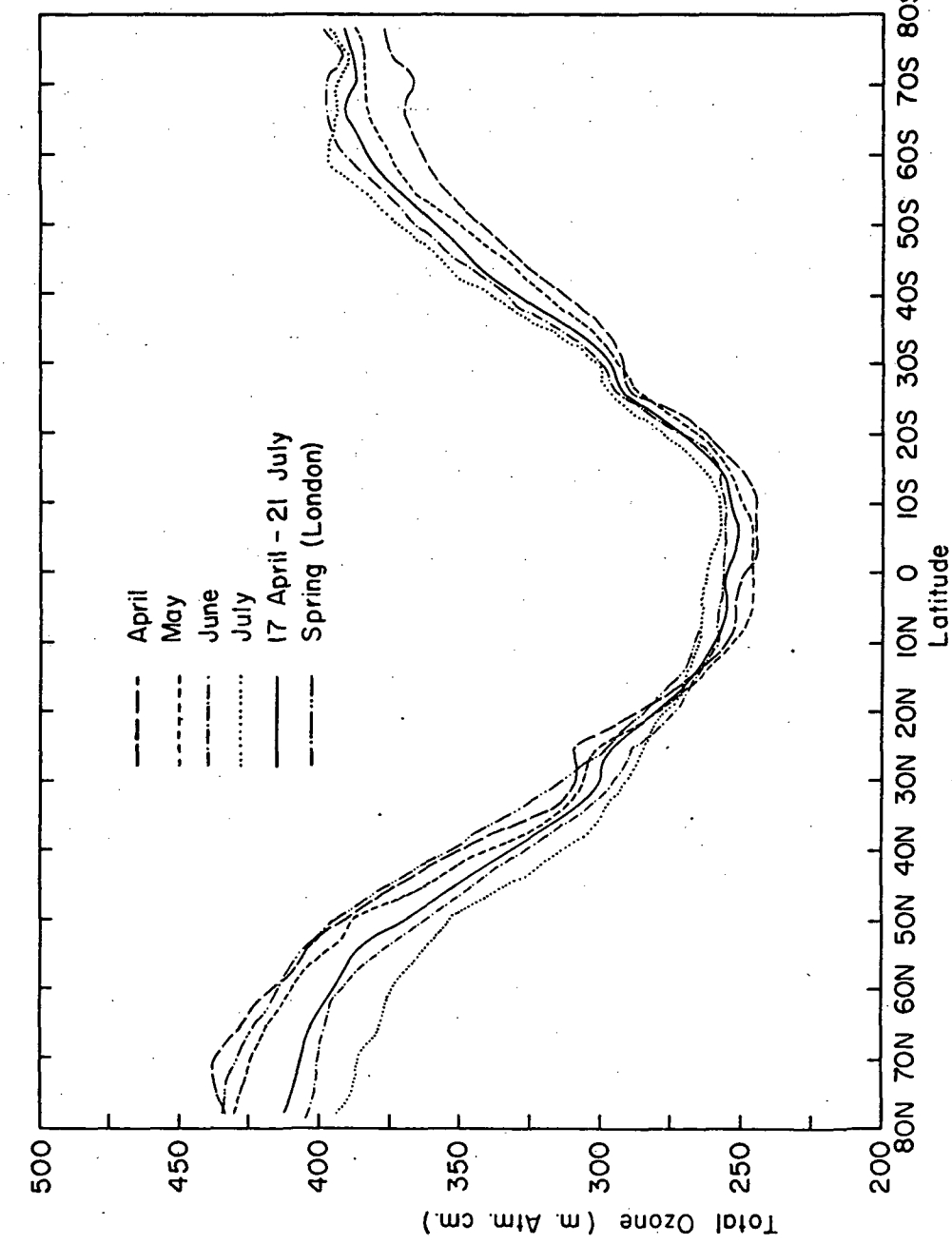

Fig. 2.126.1 Variation of total ozone with latitude and month for the Northern and Southern Hemispheres.

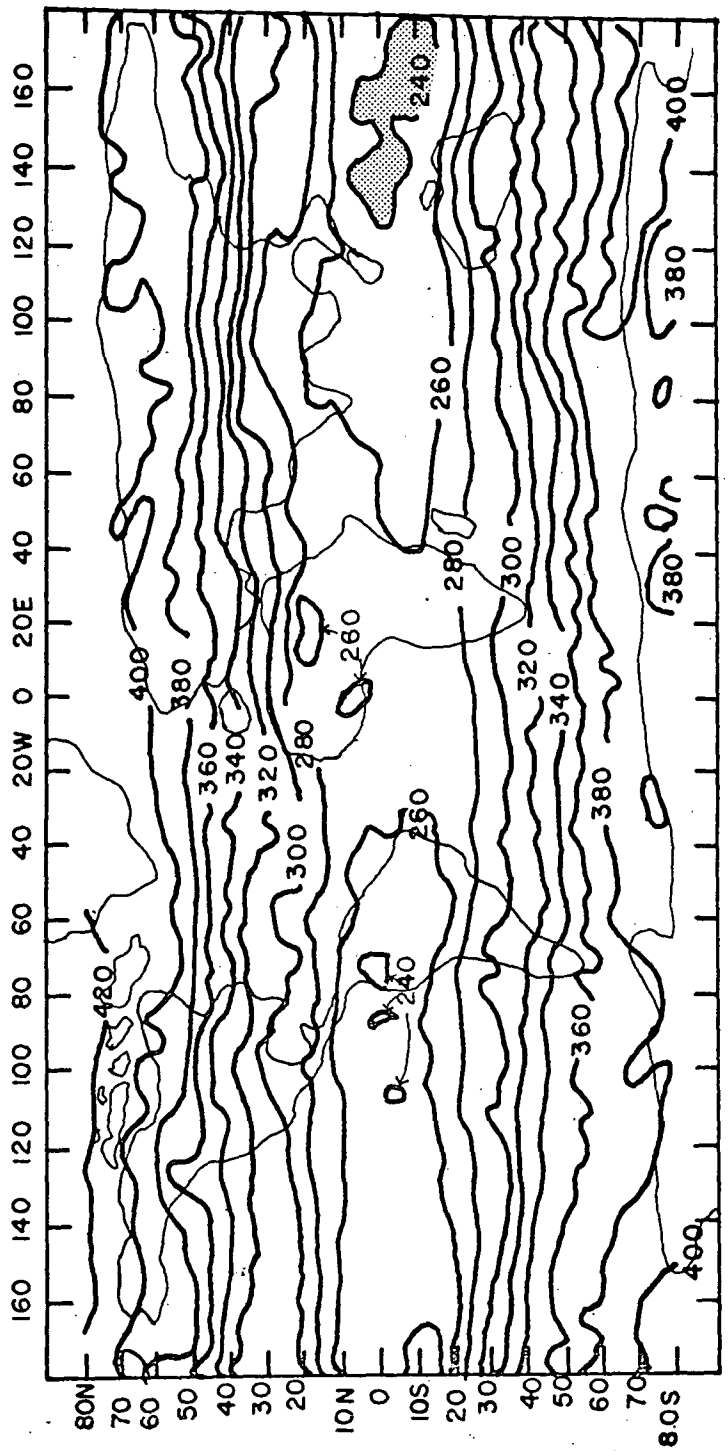

Fig. 2.127.1 Global distribution of total ozone from 19 April to 21 July 1969. A two-dimensional spline function was used to analyze 1.8×10^5 data points.

2.2 Atmospheric Thermal Structure from IRIS Spectra

All work in this area is based on IRIS radiance values archived on tapes purchased from the National Space Science Data Center. Programs to extract and analyze data were described in the semiannual report.

The goal of this effort is to obtain knowledge of the mean thermal structure of the upper troposphere and lower stratosphere over the Southern Hemisphere and to use the thermal gradients, thickness patterns, etc. derived from the radiance information to study interhemispheric circulation differences. In addition to direct use of radiance values to indirectly depict the relative thermal structure, two other approaches, regression and inversion of the IRIS data have been tested thus far.

Results and potential applications are discussed in the following subsections. They will provide information in addition, but complementary, to the ozone data.

2.21 Direct Regression of Temperature and Height Fields on Radiance

Computer programs to obtain "simultaneous" observations of temperature, height, thickness, and IRIS radiance have been completed. The purpose of these programs is to provide the observations necessary to the calculation of regression coefficients as in Smith, et al (1970). The programs screen the radiance data, eliminate obviously bad data, and eliminate those positions contaminated with clouds. The points along the satellite track that are contaminated by clouds are determined by using the radiance at 735 cm^{-1} as a check. In the presence of clouds, radiance at 735 cm^{-1}, N(735), with a weighting function peak in the low troposphere, will register less than normal. The cloud check routinely tests each point along the orbit in the 735 cm^{-1} channel against the median value of the 735 channel in a particular latitude band. If the particular location has a radiance

value less than the median value in the latitude band of that orbit by 10 egs/ or more, the point is considered cloud contaminated and eliminated. The remaining points are then smoothed over 5 points to obtain the radiance data that are compared to the conventional information from the NMC grid data. The NMC grid data are interpolated to the positions along the satellite track to finally determine the "simultaneous" observations. Tests of this method at levels throughout the upper troposphere and lower stratosphere are underway. Section 2.22 describes a method in which limited use of regression (for 100 mb temperature) aids an inversion technique.

2.22 Linear Estimation of Atmospheric Temperatures from Satellite-Observed IR Radiances

A recent paper by Rodgers (1969) gives an account of the statistical estimation of temperatures as linear combinations of weighting functions and satellite-measured IR radiances.

The radiative transfer equation for infrared radiation whose surface contribution (at the radiometer) is negligible, is

$$I(v) = \int_{p_o}^{o} B(v,p) \frac{dT}{dp} (v,p)\, dp \qquad (1)$$

where p_o is the surface pressure, p pressure-level, v wave-number, B Planck function and T transmittance.

This equation can be written as a matrix multiplication of ΔB given by

$$\Delta B = B\ (v,p) - \bar{B}\ (v,p)$$

where $\bar{B}$ represents a certain mean atmosphere, which is not the actual mean atmosphere. If the ΔB values are small the matrix transfer equation can be written in the linear form

$$\Delta I_i = I_i - \bar{I}_i = \sum_z K_{iz}\ (B_z - \bar{B}_z) \qquad (2)$$

Here K_{iz} is the weighting function for the i^{th} wave-number at level z.

When the equation is thus of a linear form, the direct mathematical solution for ΔB_z is given by

$$\Delta B_z = K_{iz}^{-1}\ \Delta I_i \qquad (3)$$

But the linearization causes the instrumental noise radiance to be comparable to ΔI_i. Thus equation (2) becomes

$$\Delta I_i = \sum_z K_{iz} \Delta B_z + e_i \qquad (4)$$

Where e_i is the instrumental noise for the i^{th} wave number.

Equation (4) has no exact solution but through estimation theory, assuming ΔI, ΔB, e_i to be distributed normally with zero means, the best estimate for B given I is obtained, which is given by

$$\Delta B^T = \Delta I^T E^{-1} K (R^{-1} + K^T E^{-1} K)^{-1} \qquad (5)$$

where E^{-1} is the inverse of the instrumental noise variance-covariance matrix, R^{-1} the inverse of the Planck function variance-covariance matrix (which is made to depend only on temperatures at different levels by making the wave number the same in all the calculations of the Planch function).

The restrictions on the use of this method are:

1. Only clear sky case temperature profiles could be obtained;

2. The R matrix is misleading unless the temperature data is from a limited geographical region and a particular period of time about which the estimation is to be made. This is because of the deviations of the ΔB distribution from the Gaussian in a more general case. This may be particularly restrictive in the Southern Hemisphere;

3. If ΔI is large compared to B_z or $\bar{B}_z$ the assumption of linearity fails and the retrieved temperatures are closer to the mean atmosphere than the actual atmosphere. This necessitates the building up of a good library of near-simultaneous radiometer-radiosonde observations.

In our actual use of the Rodgers statistical method, the retrieved temperatures deviate most from the actual temperatures near the 200 mb level in mid-latitudes. This is because of the poor correlation of the 200 mb temperatures and the radiances of the wave-numbers with weighting functions (see Fig. 2.22.1 from Conrath et al (1970)) centered near 200 mb, such as 700 cm^{-1} (Fig. 2.22.2). This should be compared with Figure 2.22.3, the scatter for 675 cm^{-1} radiances and 100 mb temperatures. Since we are interested in the meteorology of the jet stream we would like to establish the different tropopause regimes with the scatter of Figure 2.22.3, and thus use the hemispheric isotherms at the 100 mb level to obtain better temperatures in the lower levels. As related to the inversion scheme discussed, we would select a special R matrix.

Figure 2.22.3 indicates that a curvilinear fit for that scatter would be better than a linear fit. Lenear, 2nd, 3rd, and 4th degree curves were fitted to the data. The 2nd degree fit was not used since it gives very cold, unrealistic temperatures for lower radiances. The cubic fit is about the best for the data used. The temperatures derived by using this fit and the near-simultaneous NMC grid temperatures along two orbits are given (Figs. 2.22.4 and 2.22.5). The agreement is very good and the tropopause break regions are well indicated.

As is seen from Figures 2.22.4 and 2.22.5, the coldest temperatures are over the Antarctic region. These had been obtained by a linear extrapolation of the data of Figure 2.22.3. We did not have any concurrent radiosonde data to verify these temperatures. Table 2.22.1, consisting of data from Byrd Station (80.0S, 119.5W) USDC, 1968) indicated that the July average temperature near 100 mb - actually at 16Km -

for this station is about -95°C. However, Figure 2.22.6 (USDC, 1969), a climatological diagram, gives the coldest temperature in this region as -82°C which is about 23°C warmer than the more recent sounding data at Byrd. This indicates that antarctic temperatures obtained by extrapolation from Figure 2.22.3 have errors only of the order of 5°C, if the soundings are given precedence.

A map of the Southern Hemisphere 100 mb isotherms (Fig. 2.22.7) obtained by the method of the present grant indicates an extensive warm region, asymmetrically distributed over most of the 25° - 55°S belt except the Pacific and South American regions. This seems to be a very persistent feature, as we have found its presence every day over a 10 day period in early July, 1969. The mean July map (Fig. 2.22.6) shows the same smoothed relative warm area.

It is planned to investigate these and other meteorological features using 6 level temperatures and geopotential heights extending down to 700 mb. The vertical thermal structure will be obtained from our modified Rodgers method with IRIS input.

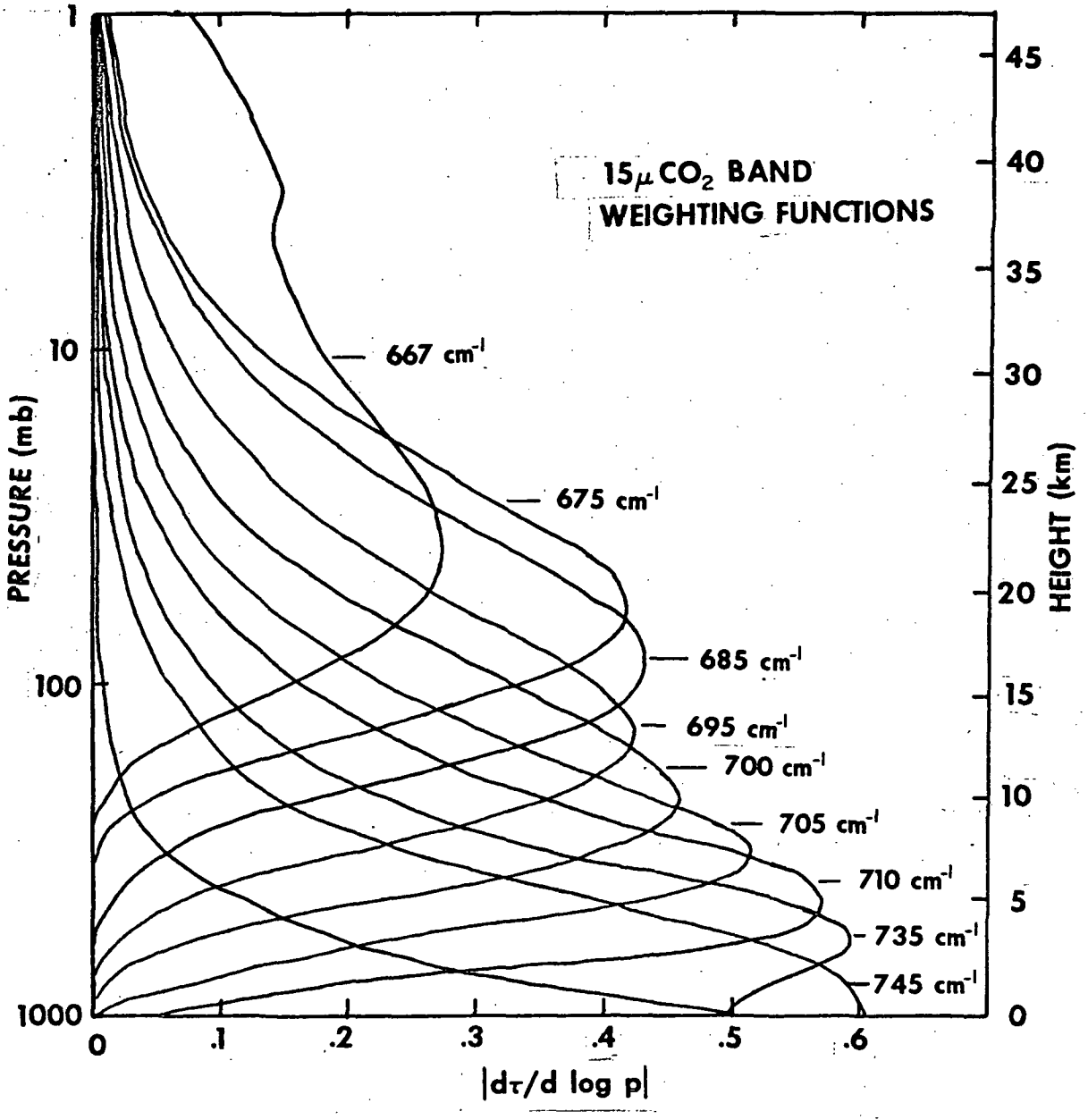

Fig. 2.22.1 Atmospheric weighting functions for 667 cm^{-1} (15μm) CO_2 absorption band. The curves were calculated assuming an instrument function 5 cm^{-1} wide at the half maximum point, centered on the wave number indicated. (After Conrath et. al., 1970)

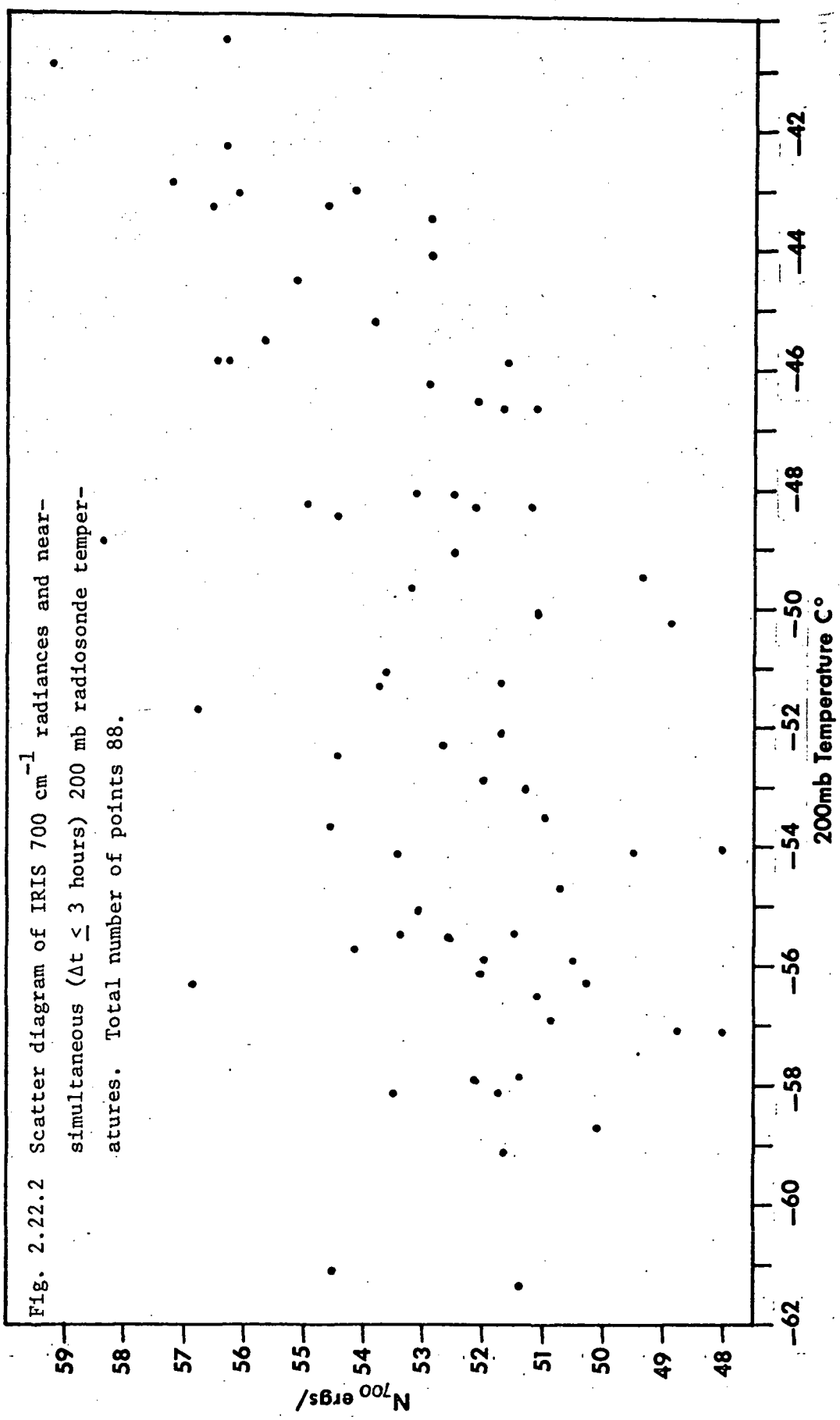

Fig. 2.22.2 Scatter diagram of IRIS 700 cm^{-1} radiances and near-simultaneous ($\Delta t \leq 3$ hours) 200 mb radiosonde temperatures. Total number of points 88.

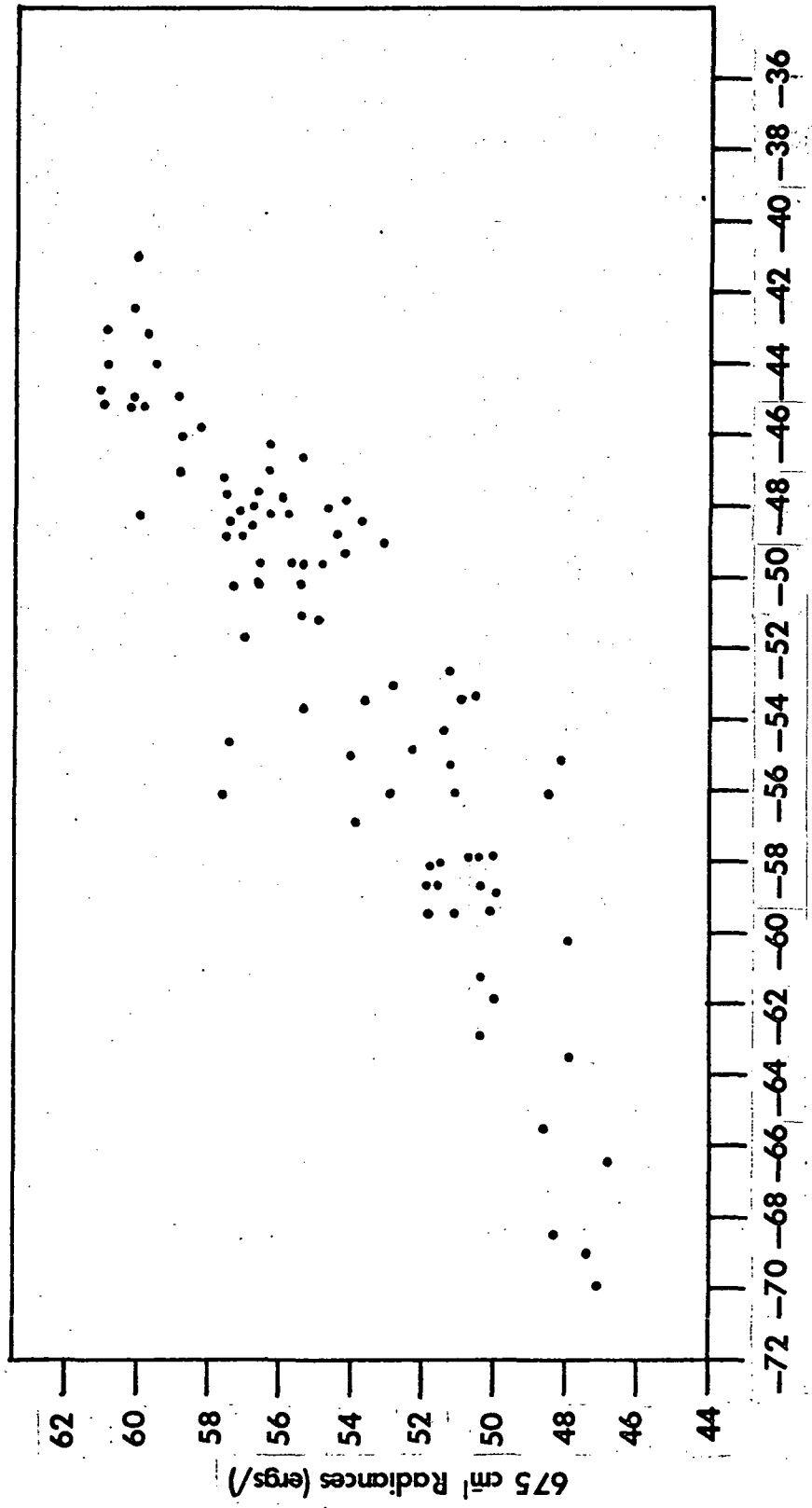

Fig. 2.22.3 Scatter of IRIS 675 cm^{-1} radiances and near-simultaneous ($\Delta t \leq 3$ hours) 100 mb radiosonde temperatures. Total number of data points 88.

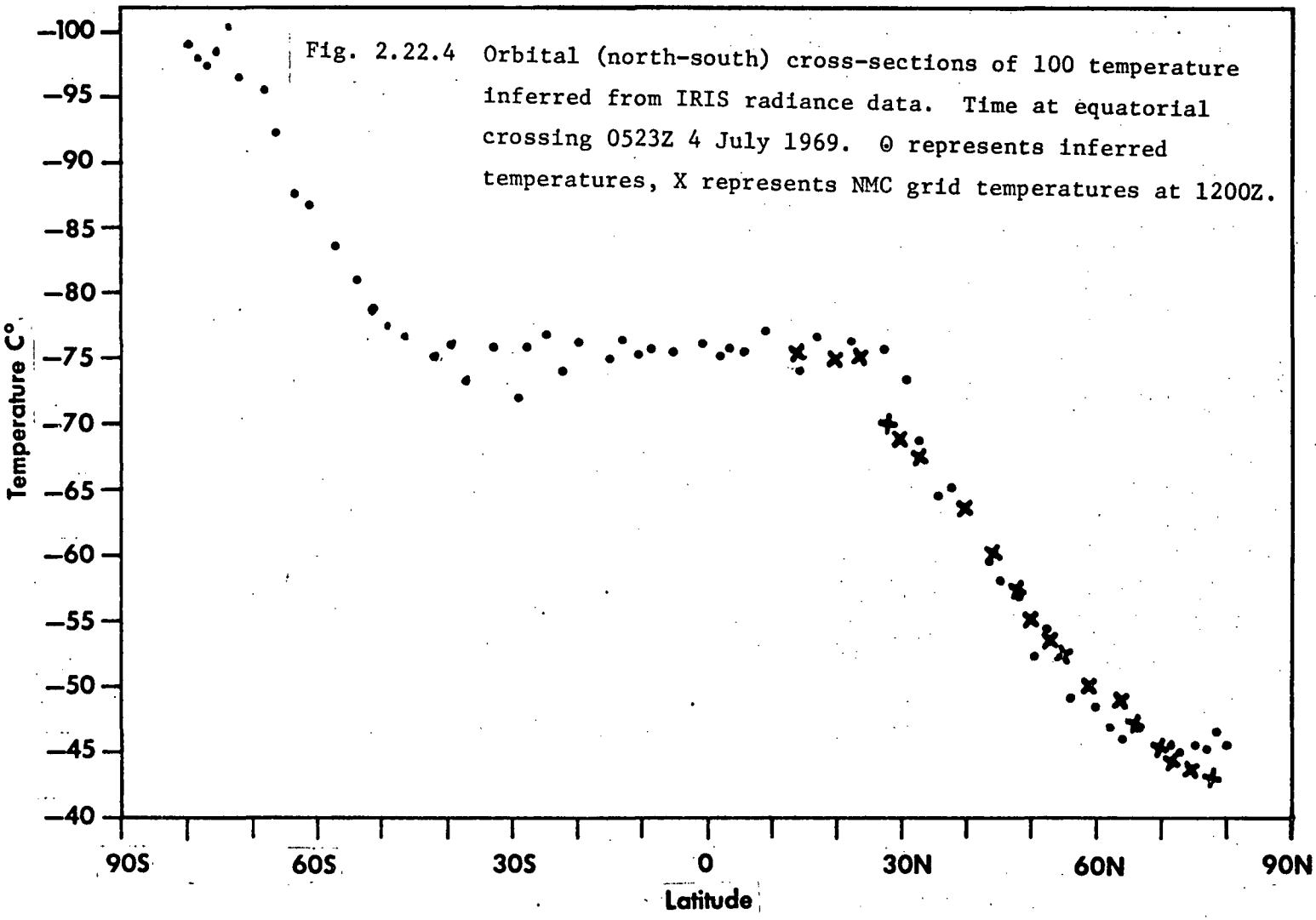

Fig. 2.22.4 Orbital (north-south) cross-sections of 100 temperature inferred from IRIS radiance data. Time at equatorial crossing 0523Z 4 July 1969. 0 represents inferred temperatures, X represents NMC grid temperatures at 1200Z.

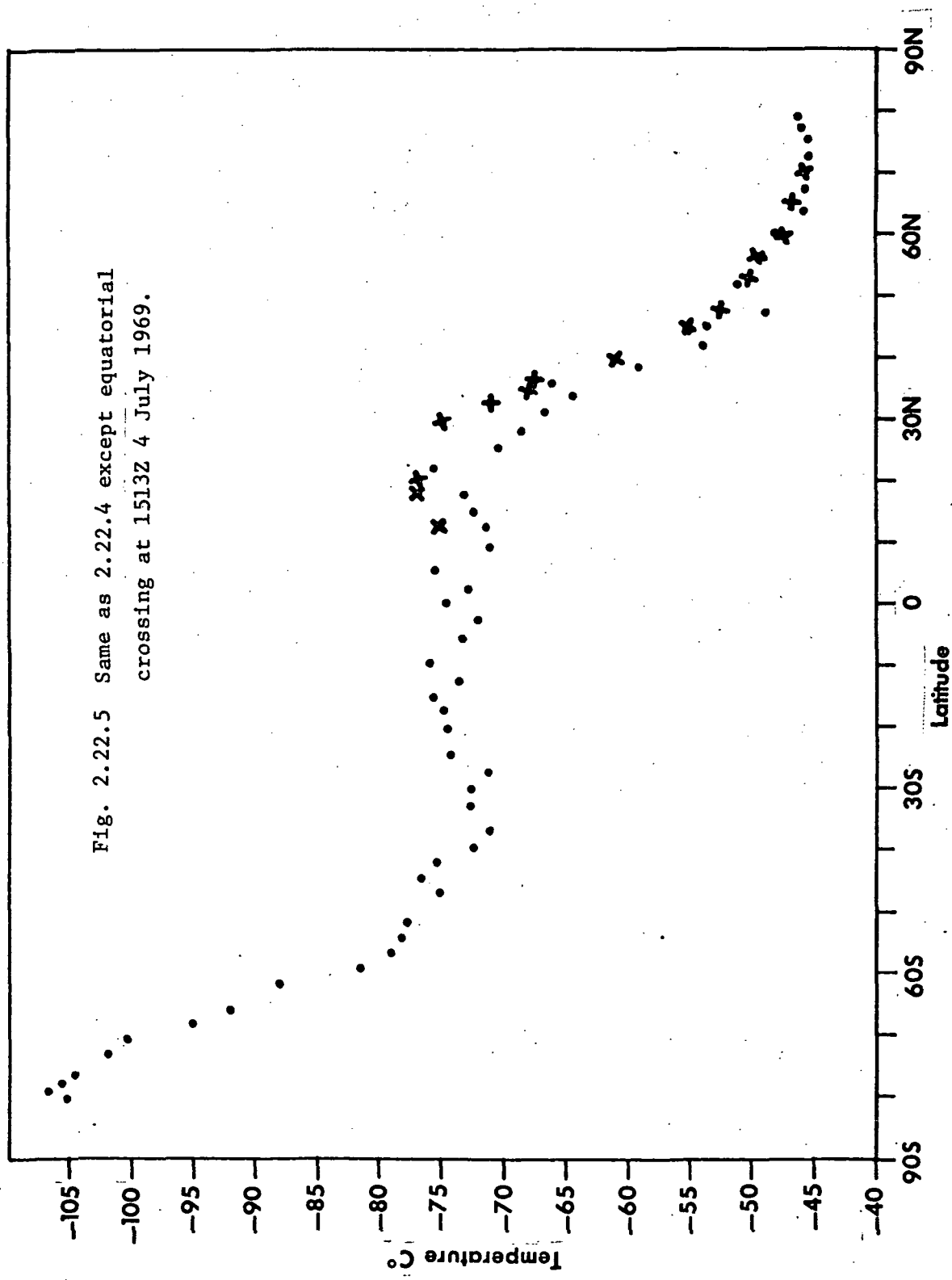

Fig. 2.22.5 Same as 2.22.4 except equatorial crossing at 1513Z 4 July 1969.

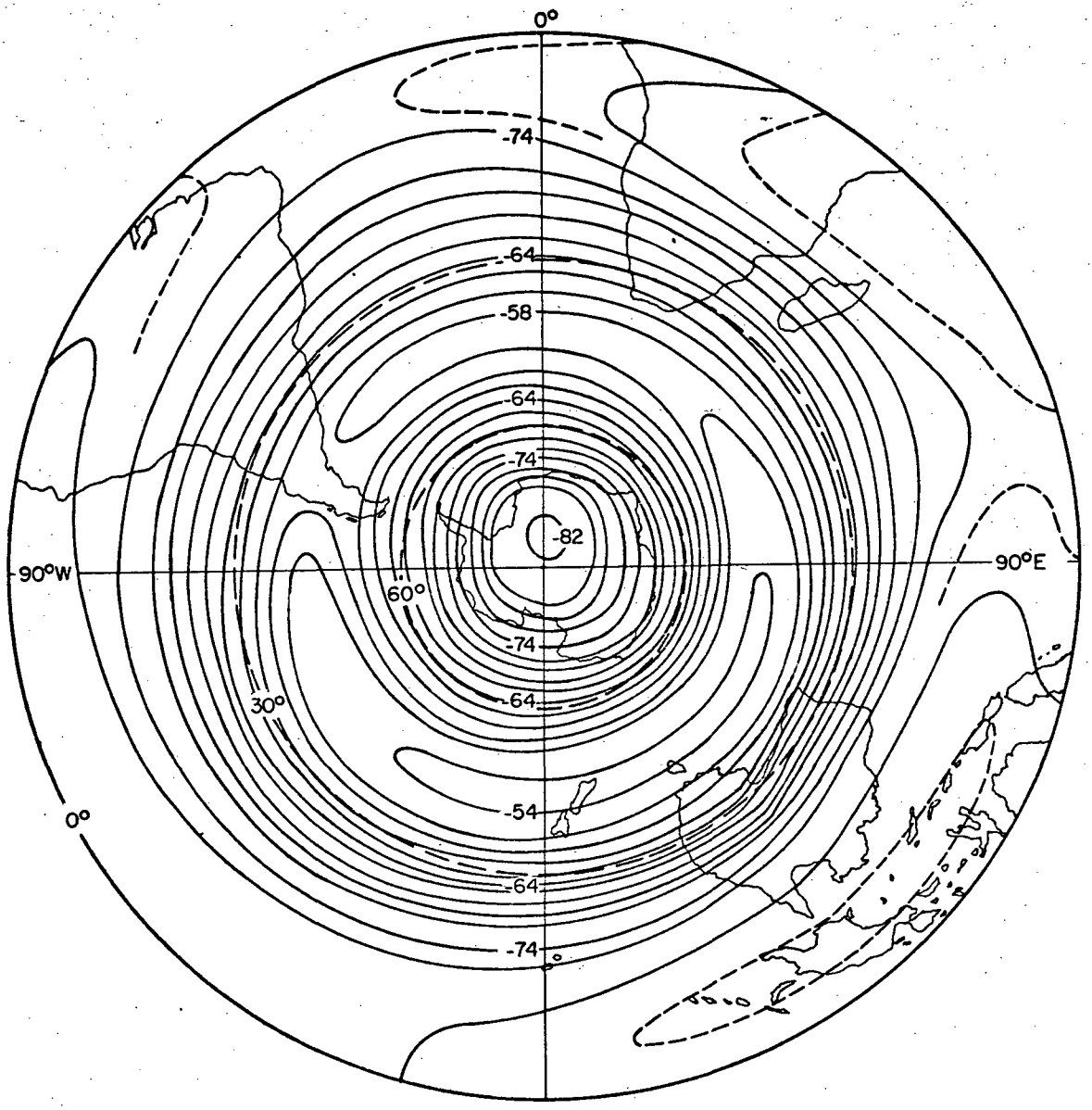

Fig. 2.22.6 Southern Hemisphere July mean 100 mb isotherms in °C. From U, S. Department of Commerce, 1969.

Table 2.22.1

16 km Temperature at Byrd Station

(80.0S, 119.5W)

DATE	TEMPERATURE ^{o}C
7-02-64	-96
7-13-64	-98
7-15-64	-97
7-17-64	-98
7-22-64	-92
7-24-64	-95
7-29-64	-97
7-07-65	-94
7-20-65	-96
7-27-65	-97
7-30-66	-82
Total	-1042
Average	$-94.7^{o}C$

Average, neglecting the 7-30-66 observation, is $-96.0^{o}C$

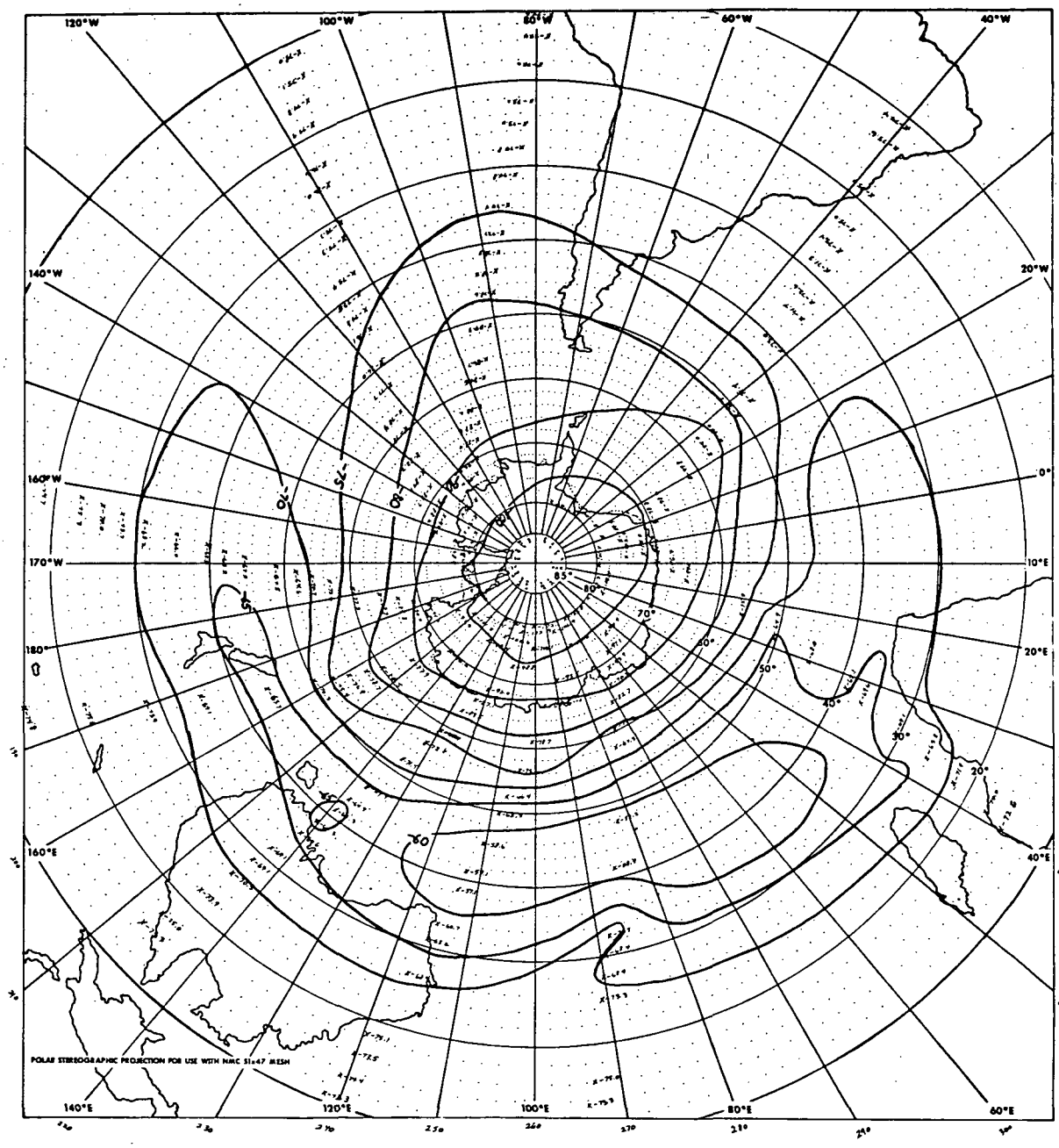

Fig. 2.22.7 Southern Hemisphere 100 mb isotherms in ^{o}C for 9 July 1969. Temperature inferred from Figure 2.22.3.

2.23 Energetics of Jet Stream Systems in the Northern and Southern Hemispheres

Section 2.121 summarized existing knowledge or differences between the general circulations of the Northern and Southern Hemispheres. Some work using total ozone derived from radiance measurements to observe differences between the hemispheres has already been accomplished and reported in Section 2.12 of this report. Temperature fields derived from IRIS data can also be used to study interhemispheric differences.

The first thing to be considered is location of jet maxima. Some work along this line has already been accomplished using O_3 meridional gradients (see Section 2.11). The temperature related channels of IRIS may also be applicable to this problem. Jet stream maxima are, of course, related to strong horizontal temperature gradients. Therefore, one might first approach a horizontal gradient of a channel radiance, say N(695), as an indicator. However, the form of the weighting functions, with significant contributions to the radiance from above and below the jet stream region may mask the intense temperature gradient of the jet. Thus, another technique has been sought. Because vertical soundings south of jet streams indicated warm troposphere and cold stratosphere and those soundings north of the jet stream have a cold troposphere and warm stratosphere a latitudinal profile of N_1-N_2 is being investigated. N_1 here is the radiance in a channel with a weighting function maximum in the middle troposphere, N_2 the radiance in a channel with a weighting function maximum in the lower stratosphere. An example is shown in Figure 2.23.1, a latitudinal profile along an orbit with the

$\Delta N = N(705)-N(685)$. Also shown is the contour height of the 250 mb surface along the satellite track as analyzed by NMC. To the north of $55^{o}N$, the ΔN is small, while to the south it is large. The break point between the high latitude and low latitude regions is around $55^{o}N$. The height profile shows that this is the approximate location of the jet. Thus, the ΔN procedure may be useful in locating jet streams. Difficulties may arise with the ΔN technique when applied to winter hemisphere data. The upper stratosphere in winter has a cold pole while the stratospheric polar vortex exists. Thus, it may be difficult to use the simple ΔN technique in winter before the breakdown of the stratosphere polar vortex. However, there appears to be ways in which the radiance data itself could be used to locate circulation features such as jet stream maxima.

With the temperatures derived from the radiance data certain parameters can be calculated which will be of interest in studying the jet stream systems of the two hemispheres and the energetics of those systems. These will include latitudinal temperature gradients, both zonally averaged and at specific longitudes, and available potential energy.

Changes in the available potential energy are closely tied to changes in kinetic energy. Under adiabatic flow conditions the sum of the available potential energy and the kinetic energy is conserved. Thus, a substantial drop over a few days in available potential energy should be related to an increase in kinetic energy. The available potential energy (a) can also be expressed as the zonal available potential energy (A_z) plus the eddy available potential energy (A_E). The expression for A is:

$$[A]_{(\lambda,\phi)} = \frac{1}{2}\int_0^{\infty} [T]_{(\lambda,\phi)} \left\{ \Gamma_d - [\Gamma]_{(\lambda,\phi)} \right\}^{-1} \left[\frac{(T)^2_{(\lambda,\phi)}}{[T]^2_{(\lambda,\phi)}} \right]_{(\lambda,\phi)} dp \qquad (1)$$

The notation follows Reiter (1969)[1]. Thus A is a function of the spatial distribution of T only.

The inter-hemispheric comparison of available potential energy and of its components A_z and A_E would be interesting from the standpoint of the "zonality" of the two hemispheres. A question may be answered as to how much of the total A is contained in A_E, on the average, in both hemispheres.

The A_E is the main source of eddy kinetic energy (K_E) in the troposphere. Wiin-Nielsen (1962) has shown that the kinetic energy can be broken up into a barotropic or mean (in the vertical) energy (K_M) and the baroclinic or shear energy (K_S). These in turn can be broken down into zonal and eddy forms. From our standpoint the shear kinetic energy is important because it can be expressed as merely a function of the temperature. This can be seen as follows. By definition:

$$K_S = \frac{1}{2g}\int_0^{p_o} \left\{ (u)^2_{(p)} + (v)^2_{(p)} \right\} dp \qquad (2)$$

where

$$(u)_{(p)} = u - [u]_{(p)} \qquad (3)$$

which is the deviation from the vertical mean $[u]_{(p)} = \frac{1}{p_o}\int_o^{p_o} u\, dp$.

1. Average values are indicated by brackets and departures therefrom by parenthesis. The ordinates along which averages and departures are computed are indicated by subscripts in parentheses.

The component u at any height can be expressed as:

$$u = u_o + \int_{p_o}^{p} \frac{\partial u}{\partial p} \, dp \tag{4}$$

where u_o - u at p_o .

From (4)

$$[u]_{(p)} = u_o + \frac{1}{p_o} \int_0^{p_o} \left(\int_{p_o}^{p} \frac{\partial u}{\partial p} \, dp \right) \, dp \quad . \tag{5}$$

Substituting (4) and (5) into (3):

$$(u)_{(p)} = \int_{p_o}^{p} \frac{\partial u}{\partial p} \, dp - \frac{1}{p_o} \int_o^{p_o} \left(\int_{p_o}^{p} \frac{\partial u}{\partial p} \, dp \right) \, dp \tag{6}$$

Using the thermal wind relation:

$$\frac{\partial u}{\partial p} = \frac{Rf}{p} \left. \frac{\partial T}{\partial y} \right|_p \tag{7}$$

$$(u)_{(p)} = Rf \int_{p_o}^{p} \frac{1}{p} \left. \frac{\partial T}{\partial y} \right|_p \, dp - \frac{Rf}{p_o} \int_o^{p_o} \left(\int_o^{p_o} \frac{1}{p} \left. \frac{\partial T}{\partial y} \right|_p \, dp \right) \, dp$$

and $(u)_{(p)}$ is a function of the spatial distribution T only.

Thus, K_S can be calculated from the three-dimensional temperature field. K_{SE} (shear kinetic energy of eddies) is also the main recipient of the conversion of A_E into kinetic energy. Changes in K_S also parallel changes in the mean or barotropic flow as seen in Figure 2.23.2. Therefore, from the radiance-derived temperatures we should be able to obtain a measure of the kinetic energy of the shear flow. This K_S can then be investigated as to temporal and spatial variations and interactions with variations of available potential energy. Also, the K_S can be

used to locate jet streams and estimate their intensity.

The possible determination of height fields via regression would enable much more complete calculations to be carried out.

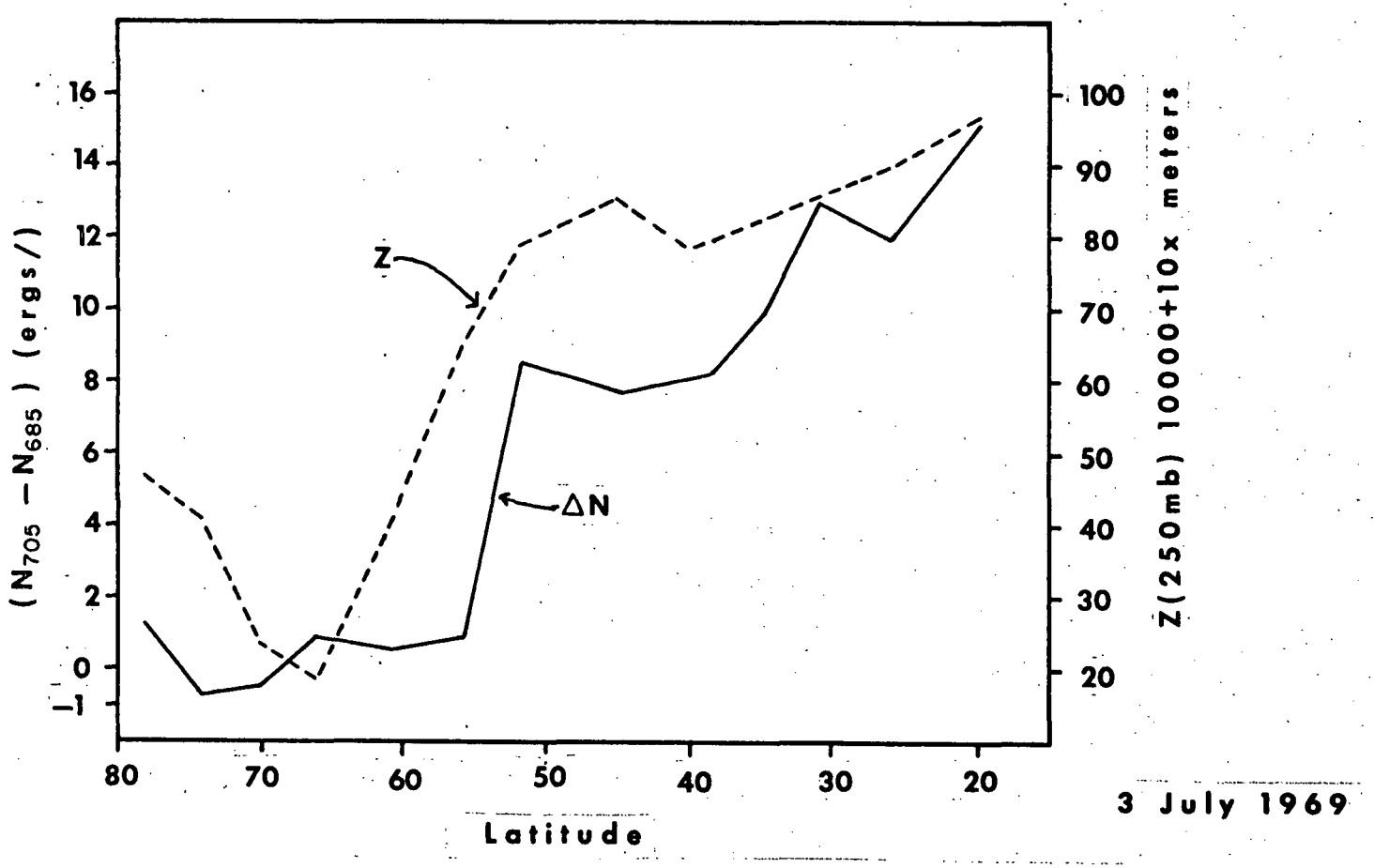

Fig. 2.23.1 Orbital profile of N(705) - N(685) and the height of the 250 mb surface.

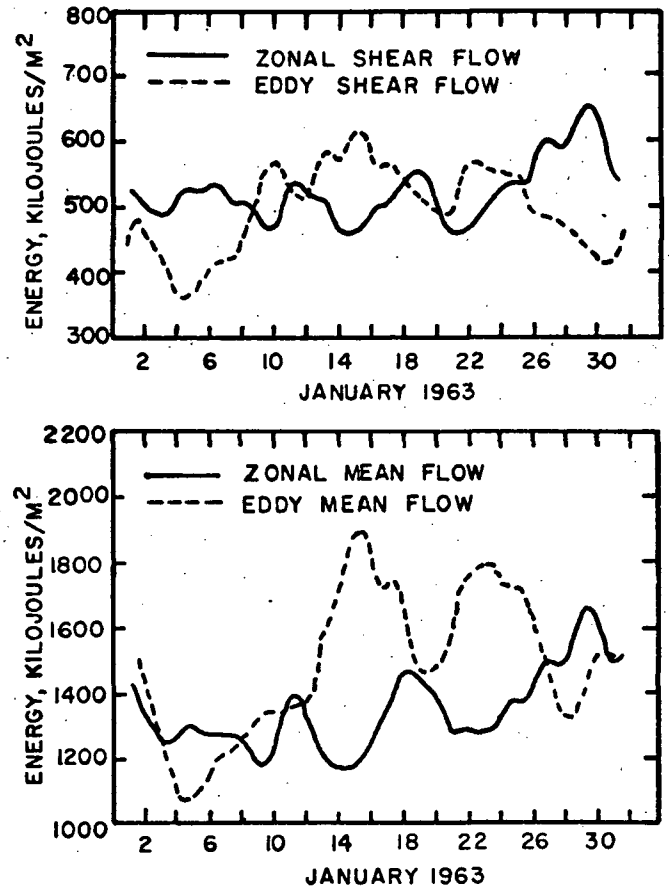

Fig. 2.23.2 Zonal and eddy shear flow and mean flow kinetic energies as functions of time during January 1963 (Wiin-Nielsen, 1965).

2.3 Statistical Characteristics of the Atmospheric Circulation in the Tropopause Regions of Both Hemispheres

Spectrum analysis of the 200 mb and 300 mb winds for 127 stations in North America and of the 30,000', 35,000' and 40,000' level winds for 10 Australian stations has been completed using data for one year and five years respectively. From such an analysis technique an indication of the relative importance of various planetary and cyclone wave regimes in tropospheric and stratospheric transport processes is obtained. The details of this investigation will provide the basis for Mr. R. F. Abbey's M. S. thesis which will be completed by the end of this year.

The determination of the statistical representatives of the mass, momentum, and energy transports derived from upper-level wind data from different geographic regions forms a major goal of this research. Only if the representativeness of such data has been established can meaningful inter- and intrahemispheric comparisons be made.

To gain more insight into hemispheric differences in atmospheric circulation, the above analysis of conventional data will be used in conjunction with the data from NIMBUS III and IV and the results derived therefrom. This procedure will not only provide a check on, and correlation between, the two types of data acquisition, but will also lend another dimension to the problem of determination of the characteristics of the general circulation of the atmosphere.

Using the spectra thus computed, various interpretations of the actual meaning of the processes which make up the respective spectra are presented. The variance distribution across North America during the data interval under consideration, 1 July 1967 - 30 June 1968, was determined (Figures 2.3.1 and 2.3.2). The 300 mb wind variances revealed a maximum area of values located in the southeast, with especially high values in the Little

Rock and Jacksonville areas. An area of minimum variance occurred in the Great Basin region to North Platte on the eastern boundary. This distribution should be expected due to the profound and distinct impact of the subtropical jet stream upon the southern United States from Texas eastward.

The axis of maximum meridional variance for the 200 mb level was orientated generally east-west with the influence of the Rocky Mountains being quite noticeable. Maximum values occurred in three regions: Oregon-Washington; southeastern South Dakota-eastern Nebraska-western Iowa; New England. It is thought that the first and third areas mentioned above are due to the shift of the long wave features of the general circulation and consequently of the storm tracks, and the second area to the perturbing influence of the Rocky Mountains upon the originally zonal current.

Each of the respective spectra were examined and the geographic distribution of spectral densities at particular frequencies was established. The quantitative results of this analysis will be contained in the M. S. thesis.

Comparisons are made between the 200 mb and 300 mb wind spectra as well as between the observations taken at 00 GMT and 12 GMT. Preliminary investigations show little difference between the 00 GMT and 12 GMT spectra as should be expected. However, this approach provided an internal check on the representativeness of the spectra compared as well as filtering out the diurnal effects which would tend to influence some of the longer period spectral values due to aliasing. Since this study is more concerned with the larger-scale motions, the above separation of spectra obviated the need to account for motions with a periodicity of less than two days.

The 200 mb and 300 mb spectra show considerable geographic differences, especially from south to north. This should be expected due to the sloping of the tropopause and the level of maximum winds from equator to pole. This particular characteristic is not as easily discernable over Australia, probably due to the sparsity of stations that could be analyzed.

Seasonal differences in the spectra were studied as well. Comparisons were made between different geographic regions using selected stations. The effect of the definition of "season" on spectra was also examined; however, further investigation in this area needs to be done before significant conclusions can be reached.

Analyses of energy generation and destruction are currently being made along the major storm tracks of North America using the area conserving spectral analyses values between selected frequencies as input data. Such analysis will show the effects of the different scales of motion in the energy processes of the general circulation.

One obvious conclusion already drawn from this study relates to the many analyses previously done along latitude circles. This study contains spectra for stations along every 4° of latitude from 20°N to 80°N as one method of partitioning the stations. By averaging the spectra along latitude circles serious misconceptions may result, and the value of using spectrum analysis as a statistical tool may be negated. Significant differences between spectra occur along any given latitude circle. The strong horizontal gradients of the kinetic energy spectra in frequency space determined in this study suggest that a regional treatment of the multivariate kinetic energy equation will have to contend with a careful evaluation of boundary flux terms.

The most significant peak to appear in the meridional spectra occurs at a periodicity of 4.93 days. Approximately 48% (55/177) of the stations analyzed exhibit a spectral peak at this frequency, (Figure 2.3.4). However, this tendency is not as strong nor as evident in the zonal spectral distribution (Figure 2.3.3). The meridional spectral densities are greater than the zonal values by almost a factor of two with the 300 mb values being greater than the 200 mb (not shown) spectral densities. All maxima are oriented from Texas to Maine indicating the most favored position for a storm track which agrees well with the "cyclone rise" found by other investigators. Figure 2.3.5 shows the mean annual position of the most favored storm tracks (after Visher, 1954).

Stations possessing a peak at 4.93 days are indicated by a square in the above figures. Most evident in the v-component distribution is the zonal band of stations with this frequency peak between 40^{o}N and 50^{o}N. This agrees favorably with the two principal cyclone tracks shown in Figure 2.3.5. The spectral distribution of the u-component of the wind shows no significant pattern with regards to stations, and has a peak value at 4.93 days.

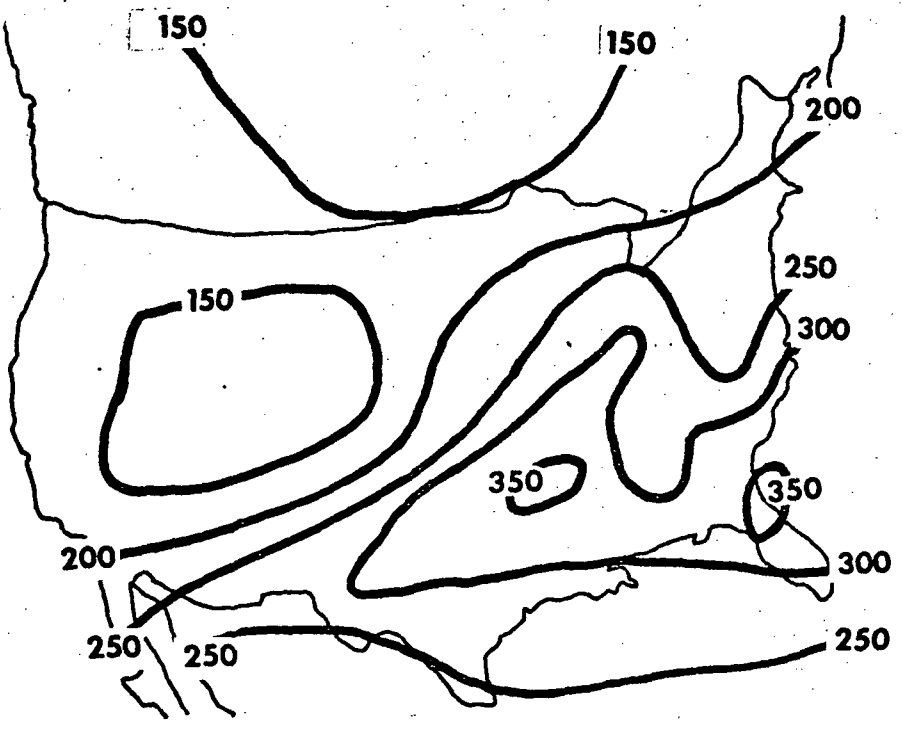

Fig. 2.3.1 U-component variance m^2/sec^2 at 200 mb for 1 July 1967 to 30 June 1968.

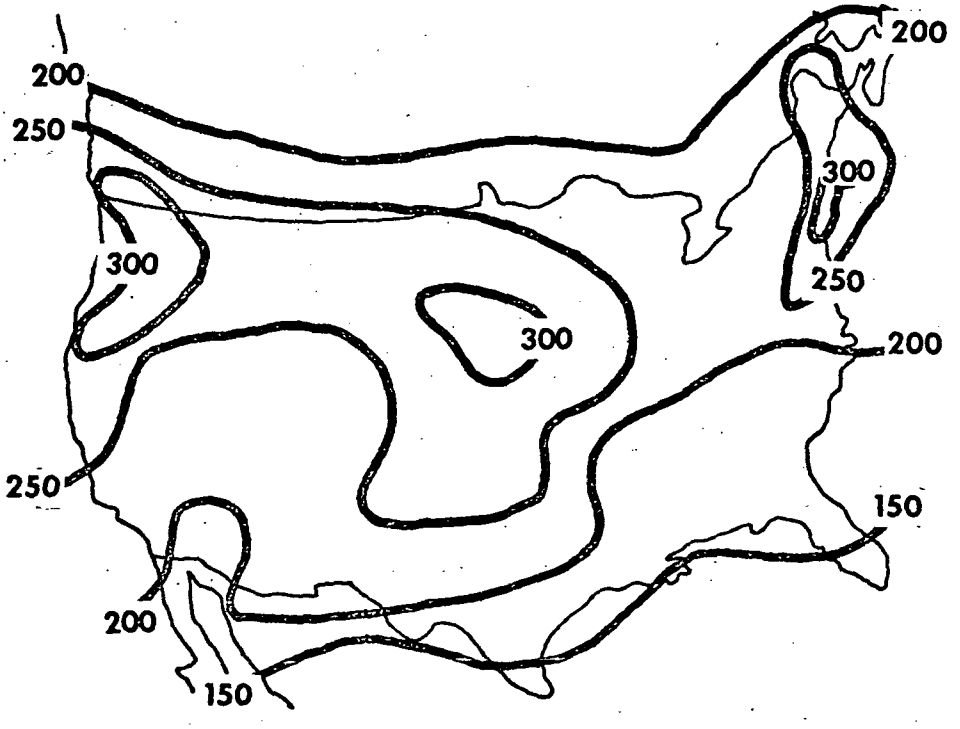

Fig. 2.3.2 V-component variance m^2/sec^2 at 200 mb for 1 July 1967 to 30 June 1968.

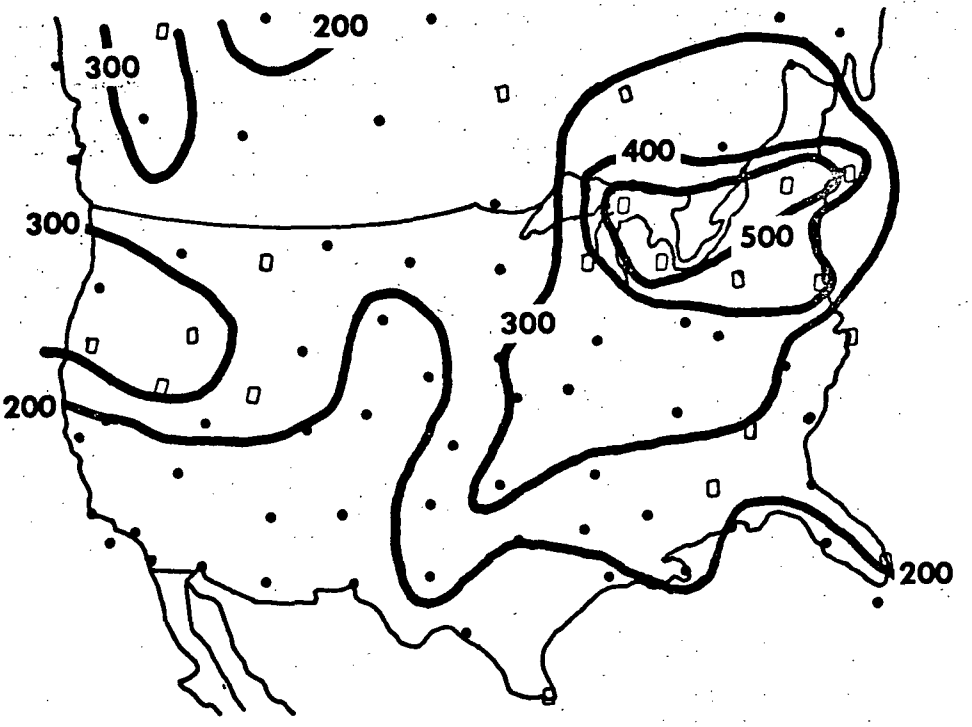

Fig. 2.3.3 U-component spectral density (non-normalized) [$M^2/sec^2/day$] for 300 mb 00Z at a period of 4.93

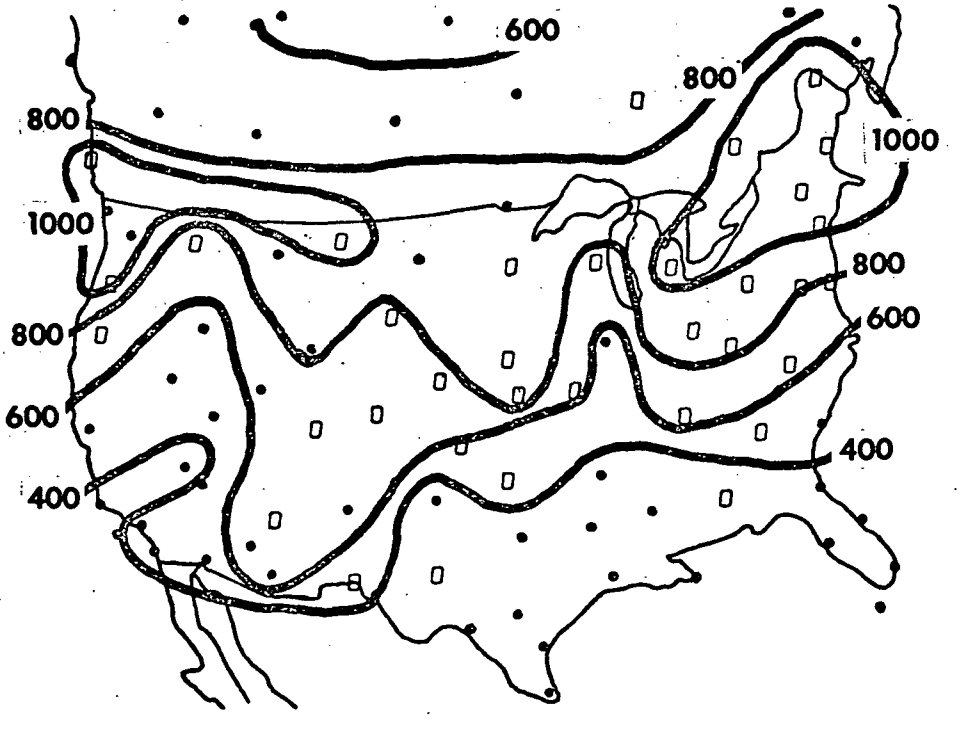

Fig. 2.3.4 Same as 2.3.3 except v-component.

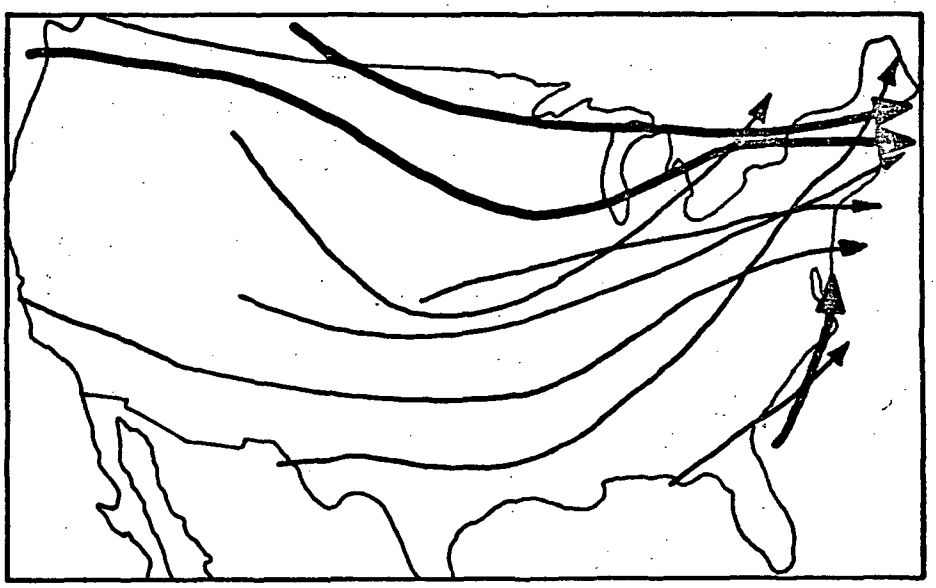

Fig. 2.3.5 Tracks taken by many lows; width of line suggests relative abundance. (From Visher, 1954).

3.0 Program for Next Reporting Period

The research results reported in the foregoing chapters encourage us to probe deeper into the detailed structure of the upper troposphere and stratosphere, making extensive use of NIMBUS radiance data. Meridional gradients in total ozone as well as in radiance-derived temperatures were mentioned as first indicators of the presence of jet maxima. Our knowledge of the structure and dynamics of jet streams (see e.g. Reiter, 1963, Jet Stream Meteorology, Chapter in World Survey of Climatology, Vol. 4) has not yet been employed to its fullest extent in "massaging" the available satellite data without introducing statistical bias. Above all, we will have to search for optimum techniques that will depict and differentiate between the polar front and subtropical jet stream systems of middle latitudes, and the easterly jet stream of the tropics, which is found only during the summer and in the African and Asian longitude sectors. The latter jet stream system with its wide-spread cloudiness and monsoonal precipitation systems may not be easy to detect from radiance data with our present analysis techniques.

We intend to make a special effort on retrieving "unorthodox" auxiliary data from the Southern Hemisphere, such as GHOST and EOLE balloons trajectories. Such data may help in verifying the position of long-wave troughs and ridges in otherwise data-sparse regions.

Some of the preliminary results reported,especially on the correlation between ozone gradients and jet stream intensities, will have to be tested against independent data samples, possibly from different seasons. If the conclusions that may be drawn, for instance, from Figure 2.11.1, can be generalized, they may well afford us with a diagnostic tool that

could be put to use for the planning and execution of flight operations in the Southern Hemisphere. An estimate of jet stream winds, together with cloud distributions from standard satellite surveillance, would enhance appreciably the capabilities of aviation meteorology and of weather forecasting in regions void of radiosonde data.

4.0 Conclusions and Recommendations

The encouraging results obtained during the past contract period warrant an extension of our investigations to additional time periods. It becomes desirable to obtain as nearly as possible one full year of IRIS data in order to achieve a global ozone study for all seasons of both hemispheres. Especially the question of differences in the seasonal behavior of the jet stream system in the Northern and Southern Hemispheres, should be explored more fully with such a data bank.

The study on temperature and height fields obtained from radiance data, as well as the investigation of atmospheric energetics in both hemispheres, will depend on a complete data set that extends over all four seasons.

The computer programs established during the past contract period will facilitate the reduction and analysis of satellite data, so that our research will progress at an accelerated pace.

5.0 REFERENCES

Conrath, B. J., R. A. Hanel, V. G. Kunde and C. Prabhakara, 1970: The infrared interferometer experiment on NIMBUS III. Goddard Space Flight Center, Greenbelt, Maryland

Craig, R. A., 1965: The upper atmosphere. Meteorology and physics. International Geophysics Series, Vol. 8, Academic Press, Inc., New York

Fritz, S., 1970: Earth's radiation to space at 15 microns: Stratospheric temperature. J. Appl. Meteor., 9(10): 815-824

Kao, S.-K. and W. P. Hurley, 1962: Variations of the kinetic energy of large-scale eddy currents in relation to the jet streams. J. Geophys. Res., 71(18): 4289-4296

London, J., 1963: The distribution of total ozone in the Northern Hemisphere. Beitr. Phys. Atmos., 36: 254-263

Loon, H. van, 1964: Mid-season average zonal winds at sea level and at 500 mb south of 25 degrees south, and a brief comparison with the Northern Hemisphere. J. Appl. Meteor., 3

_____, 1965: A climatological study of the atmospheric circulation in the Southern Hemisphere during the IGY, part I: 1 July 1957 - 31 March 1958. J. Appl. Math., 4

Lovill, J. R. and A. Miller, 1968: The vertical distribution of ozone over the San Francisco Bay area. J. Geophys. Res., 73(16): 5073-5079

Obasi, G. O. P., 1963a: Poleward flux of atmospheric angular momentum in the Southern Hemisphere. J. Atmos. Sci., 20(6): 516-528

_____, 1963b: Atmospheric momentum and energy calculations for the Southern Hemisphere during the IGY, Scientific Report No. 6. MIT

Reed, R. J., J. L. Wolfe and H. Nishimoto, 1963: A spectral analysis of the energetics of the stratospheric sudden warming of early 1957. J. Atmos. Sci., 20

Reiter, E. R., 1963: Jet stream meteorology. The University of Chicago Press, Chicago

_____, 1969: Atmospheric transport processes, part 1: Energy transfers and transformations, AEC critical review series. U. S. Atomic Energy Commission, Division of Technical Information, Oak Ridge, Tennessee

_____, 1970: Semiannual report for Grant NGR 06-002-098. Colorado State University

_____, 1971: Atmospheric transport processes, part 2: Chemical tracers. AEC Critical review series. U. S. Atomic Energy Commission, Division of Technical Information, Oak Ridge, Tennessee

Rodgers, C. D., 1969: Remote sounding of the atmospheric temperature profile in the presence of clouds. Clarendon Laboratory, Oxford, England

Scherhag, R., 1969a: 100, 200, and 300 mb contour charts. Meteorologische Abhawdlunger, 101 (4), Institute Fur Meteorologie und Geophysik der Freien Universitat Berlin

_____, 1969b: 100, 200, and 300 mb contour charts. Meteorologische Abhawdlunger, 101 (6), Institute Fur Meteorologie und Geophysik der Freien Universitat Berlin

Smith, W. L., H. M. Woolf and W. J. Jacob, 1970: A regression method for obtaining real-time temperature and geopotential height profiles from satellite spectrometer measurements and its application to NIMBUS III "SIRS" observations. Mon. Wea. Rev., 98(8)

Starr, V. P. and R. E. Dickinson, 1963: Large-scale vertical eddies in the atmosphere and the energy of the mean zonal flow. Geophis. Pura. Appl., 55, 133-136

Teweles, S., 1964: Stratospheric-mesospheric circulation, Research in Geophysics, Vol. 2. H. Odishaw (ed.), 509-528, MIT Press, Cambridge, Mass.

United States Department of Commerce, ESSA, Environmental Data Service, 1969: Climate of the upper air, Southern Hemisphere, Vol. 1 - Temperatures, dew points, and heights at selected pressure levels.

United States Department of Commerce, ESSA, 1968: Ozonesonde observations 1962-1966. ESSA Research Laboratories, ERL 80-APCL 3

Visher, S., 1954: Climatic Atlas of the United States. Harvard University Press, Cambridge, Mass.

Wiin-Nielsen, A., 1962: On transformation of kinetic energy between the vertical shear flow and the vertical mean flow in the atmosphere. Mon. Wea. Rev., 90(8): 311-323

Wiin-Nielsen, A., 1965: New observational studies of energy and energy transformations in the atmosphere. Proceedings of the symposium on research and development aspects of long-range forecasting. Tech. Note No. 66, 177-202, WMO

Wooldridge, G., and E. R. Reiter, 1970: Large scale atmospheric circulation characteristics as evident from GHOST balloon data. J. Atmos. Sci., 27(2), 183-194